

Chapter 7

THE CHARGING OF SPACECRAFT SURFACES

H.B. Garrett

The buildup of static charge on satellite surfaces is an important issue in the utilization of satellite systems. The analysis of this spacecraft environmental interaction has required important advances in basic charging theory and the development of complex codes to evaluate the plasma sheaths that surround satellites. The results of these theories and calculations have wide application in space physics in the design of systems and in the interpretation of low energy plasma measurements.

In this chapter, those aspects of charge buildup on satellite surfaces relevant to the space physics community are summarized. The types of charging processes, models of charge buildup, satellite sheath theories, and charging observations are described with emphasis on basic concepts.

As many books and monographs on specific aspects of the charging of bodies in space have appeared in the last two decades, it is difficult to cover all areas in detail in a chapter of this nature. Rather, the chapter is limited to the charging of spacecraft surfaces in the near-earth magnetosphere. Rocket measurements are only briefly treated. The reader is referred to books by Singer [1965], Grard [1973a], Rosen [1976], Pike and Lovell [1977], and Finke and Pike [1979] that contain papers on the charging of natural bodies such as the moon [Manka, 1973; Freeman et al., 1973], dust particles [Feuerbacher et al., 1973] and other planetary bodies [Shawhan et al., 1973]. A brief historical review of spacecraft charging is followed by a discussion of observations. Following a description of the major charging mechanisms, specific spacecraft charging models are examined with emphasis on basic concepts. A substorm worst case environment is included. The chapter concludes with a discussion of spacecraft charge mitigation techniques. A more detailed version of this chapter can be found in Garrett [1981].

7.1 SPACECRAFT CHARGING HISTORICAL PERSPECTIVE

The historical roots of spacecraft charging analysis can be traced to the early electrostatic probe work of Langmuir [Langmuir, 1924; Mott-Smith and Langmuir, 1926]. Not only is the Langmuir probe still an important space plasma instrument, but as will be discussed, much of Langmuir's

analysis is applicable to current spacecraft charging problems. This is true as in a very real sense the space vehicle itself can be considered as a "floating probe." This theme, of the vehicle as a probe, will form the basis of much of this chapter.

Probe theory has developed into an important subfield of plasma physics in its own right, see review by Chen [1965]. It has only been with the advent of rockets and ultimately satellites that the charging of objects in space has become a major separate area of concern. The first period of charging studies, in fact, was concerned with the potential of interstellar dust grains. One of the earliest studies, that of Jung [1937], found that photoemission and electron accumulation were probably the dominant processes in interstellar space. This subject was extended and put on a firm physical footing by Spitzer [1941; 1948], Spitzer and Savedoff [1950], and others [Cernuschi, 1947; Opik, 1956]. Depending on the assumed "sticking" probability of the electrons, the photoemission yield, and the ambient environment, the estimate satellite to space potentials for these early studies ranged between -3 and $+10$ V.

With the advent of rocket-borne sensors in the early 1950s, spacecraft charging emerged as a discipline. Perhaps the first example of a spacecraft charging effect is in a paper by Johnson and Meadows [1955]. They theorized that shifts in the ion peaks measured by their RF mass spectrometer above 124 km could be explained by a negative rocket potential of -20 V. The first treatment of the charging of a macroscopic object was published the next year by Lehnert [1956] who estimated satellite to space potentials of -0.7 to -1.0 V when ion ram effects were included.

Not only did 1957 see the launch of Sputnik, but it ushered in a second phase in spacecraft charging studies. Gringauz and Zelikman [1958] discussed the distribution of charge (or sheath) around a space vehicle in the ionosphere and the influence of photoemission and satellite velocity. Jastrow and Pearse [1957], while neglecting photoemission but including ram effects, computed the drag on a satellite caused by charged particles in the ionosphere. Their study for the ionosphere assumed $T_E \gg T_I$ so that the estimated potentials were between -10 V (night) and -60 V (day), values which are too high as $T_E \approx T_I$ is the actual case [Brundin, 1963]. Another basic assumption of their study, as in the related study of Chang and Smith [1960], is that

CHAPTER 7

the ion density is little changed in the immediate vicinity of the vehicle.

Zonov [1959] and Beard and Johnson [1960] analyzed the effects of electric fields induced by the movement of a satellite across the earth's magnetic field; these fields can be quite important for large structures. Beard and Johnson [1961] also discussed the effects of emitting charged particles from a vehicle and the limitations on vehicle potential in the ionosphere, another issue which is still of concern (see Section 7.4.1). In the same period, the first satellite potential measurements were made by Sputnik 3. Krassovsky [1959] found a potential of -6.4 V and $T_E = 15$ 000 K at 795 km.

The first review of spacecraft charging appeared in 1961 [Chopra, 1961]. Despite difficulties with this review (Chopra predicted high positive potentials since the photoelectron flux he assumed was too high), it can be used as a convenient marker for the end of the second phase of the study of spacecraft charging. By 1961 most of the elements of current spacecraft charging theory were in place. Preliminary observations by rockets and satellites had confirmed that charging existed and, in agreement with some theories, was on the order of a volt (typically negative) in the ionosphere. Photoemission and the ambient electron flux were recognized as dominant sources and $\mathbf{v} \times \mathbf{B}$ effects had also been considered. On the negative side, secondary emission and backscatter had not really been adequately considered [Whipple, 1965], charged particle drag (which was ultimately shown to be of less importance than errors in the neutral drag coefficient (see reviews by Brundin [1963] and deLeeuw [1967])) was still of primary concern, and self-consistent solutions of the particle trajectories and fields had not been carried out. Only monoenergetic or Maxwellian distributions were being considered.

The new phase of studies in spacecraft charging actually started somewhat earlier than 1961 with Bernstein and Rabinowitz's probe study. Bernstein and Rabinowitz [1959] introduced a means of calculating particle trajectories in the vicinity of a probe for the case where collisions could be ignored. The importance of their study (see Section 7.4.4) was that their method allowed a self-consistent solution of the time-independent Vlasov equation and Poisson's equation. Their work was later adapted to spacecraft by a number of investigators. Davis and Harris [1961], by a more simplified method, calculated the shielding of a rapidly moving sphere in the ionosphere by estimating ion trajectories in a fixed electron sheath. Their results concerning the distribution of ions in the wake, despite their neglecting the ion thermal velocity, are consistent with Explorer 8 measurements reported in the same year [Bourdeau et al., 1961]. These latter results are probably the first accurate spacecraft potential measurements between 425 km and 2300 km. The ion current, which varied strongly as a function of angle relative to the satellite velocity vector, was found to agree with Whipple's [1959] theory (see Equation (7.23)). A satellite potential of -0.15 V was observed along with $\mathbf{v} \times \mathbf{B}$

effects (~ 0.14 V). During this period more believable potential measurements were also reported for rocket probes as exemplified by Sagalyn et al. [1963] who found potentials of -0.4 V (150 km) to -1.7 V (450 km).

In a 1961 paper, Kurt and Moroz [1961] predicted potentials of -3.2 to 4 V outside the radiation belts. They also predicted potentials as high as -20 kV in the radiation belts. Although only crude estimates, their predictions anticipated the -20 kV potentials observed in eclipse on the geosynchronous ATS 6 satellite in the 1970s. These and other results were compared in an excellent review of the effects of charged particles on a satellite by Brundin [1963]. Another good review from this period, in which the validity of various ionospheric measurements were discussed, is that of Bourdeau [1963]. The most complete works of this period, however, are in the first book concerned with spacecraft charging [Singer, 1965] and the thesis of Whipple [1965]. Whipple's thesis brings together most of the preceding results in an analysis of the roles that secondary emission, backscatter, photoemission, and magnetic field effects have in spacecraft charging. As such, it completes the third period of spacecraft charge analysis—a period marked by a realization of the importance of spacecraft charging for plasma measurements and of the importance of self-consistent calculations. Quantitative measurements also became available for the first time. The period 1965 to the present has been primarily one of refinement and extension of these 1961–1965 results to higher altitude regimes and more complex geometric situations. It represents the “fourth period” of spacecraft charging and is the concern of this chapter.

7.2 SPACECRAFT CHARGING OBSERVATIONS

7.2.1 Rocket Measurements

Rocket measurements of the ionospheric plasma have been routine since the early 1950s. The first observations of spacecraft potentials were probably the RF spectrometer measurements on a rocket by Johnson and Meadows [1955]. They made use of the differences in the energy shifts of different ionized species to estimate a vehicle potential of -20 V above 120 km. Sagalyn et al. [1963], employing 2 spherical electrostatic analyzers mounted on a Thor rocket, found much lower potentials of -0.4 V (150 km) to -1.7 V (450 km). Their measurements are in good agreement with subsequent satellite measurements in the same region. Narcisi et al. [1968] also found rocket potentials of about -0.5 V in the D and E regions although their results may have been affected by the potential distribution near the rocket [Parker and Whipple, 1970]. As discussed by Parker and Whipple [1970], however, there are for these and similar satellite measurements difficulties in interpreting the results

CHARGING OF SPACECRAFT SURFACES

since the detailed particle trajectories must be considered in determining the actual instrument responses. Further, as probably happened to Johnson and Meadows [1955], the electric fields near the rockets may be perturbed by exposed potential surfaces. See, for example, the results of the recent "tethered payload" experiment of Williamson et al. [1980], in which a potential of +10 V on the main payload induced a potential of -5 V on the secondary payload 40 m away.

Olsen [1980] (see also Winckler [1980]) has described potential measurements from a number of rocket beam experiments. These ranged from the Aerobee flight [Hess, 1969] through the Echo series [Hendrickson, 1972; Winckler, 1976] down to the recent ARAKS [Cambou et al., 1978], Precede, and Excede [O'Neil et al., 1978a, and b]. Although extensive literature exists on many of these flights, the majority is concerned with the beam aspects. Potentials, when observed, were typically a few tens of volts positive or negative relative to the ambient plasma (Jacobsen and Maynard [1980], however, have reported potentials of hundreds of volts on the POLAR 5 rocket experiment). As an example, voltages of +4 V (108 km) to +28 V (122 km) were observed by Precede (electron beam voltage: ~2.5 kV; current: ~0.8 A O'Neil et al., [1978a]).

An exception to the rocket beam flights just mentioned was the "Spacecraft Charging Sounding Rocket Payload" [Cohen et al., 1979; Mizera et al., 1979]. This flight tested prototypes of the positive and negative charge ejection systems, the transient pulse monitor, and the rocket surface potential monitor subsequently flown on the P78-2 SCATHA satellite. Additionally, a thermal emissive probe, a bipolar-intersegment voltmeter, and a retarding potential analyzer were also flown. The unneutralized beams repeatedly varied the rocket ground potential between -600 V and +100 V (Figure 7-1, Cohen et al. [1979]). Potentials as high as +1100 V were observed on conducting surfaces and +400 V on insulators [Mizera et al., 1979] relative to spacecraft ground. The variations in the vehicle to space potential correlated well with the ambient plasma density.

7.2.2 Satellite Measurements

Satellite measurements at low earth orbit have been made primarily by retarding potential analyzers and similar current collection probes. The earliest satellite observations of spacecraft charging were by the ion trap experiment on Sputnik 3 which measured potentials in the -2 V to -7 V range [Krassovsky, 1959]; however, Whipple [1959] estimated -3.9 V. As has been discussed, the first well documented measurements of satellite potential at low altitudes were by the Explorer 8 where potentials of -0.15 V were observed between 425 and 2300 km [Bourdeau et al., 1961]. Such low negative values are typical of this region: Reddy et al. [1967], -0.5 V at 640 km on TIROS 7; Samir [1973], -0.71 V to -0.91 V between 600 and 900 km (Explorer 31); Goldan et al. [1973], -0.7 V between 400 and 650

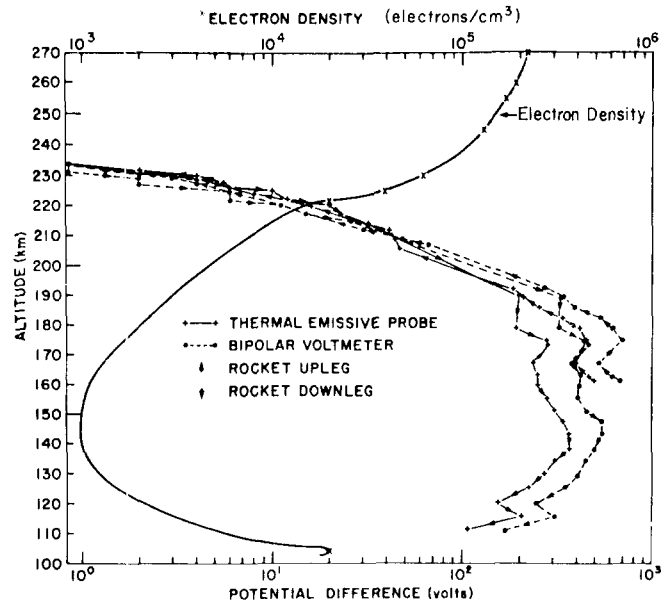


Figure 7-1. Vehicle-to-ambient potential difference and electron density (modeled) as a function of altitude [Cohen et al., 1979].

km (OGO 4); Sagalyn and Burke [1977], -1.5 V to 4 V in the plasma trough and -0.5 to -1 V in the polar cap at 2500 km (INJUN 5); and Samir et al. [1979 a, b], -0.1 to -1.3 between 275 to 600 km (AE-C). The highest values observed at low altitudes were by Hanson et al. [1964; 1970] who estimated potentials of -6 V at 240 km to -16 V at 540 km and Knudsen and Sharp [1967] who recorded -15 V at 516 km. Even higher values of -40 V were observed by Sagalyn and Burke [1977] at 2500 km on INJUN 5. These latter values are probably valid as they were observed in the auroral zone during impulsive precipitation events and at night. Although most of these results were for eclipse conditions, there was no unambiguous effect due to photoelectrons at these altitudes (this is not true for higher altitudes).

Higher voltage variations, particularly in sunlight, are seen in the plasmasphere proper at altitudes above 2500 km. On OGO 5, Norman and Freeman [1973] found potentials of -7 to -10 V at 1.1 R_E . Between 2 to 6 R_E , as the satellite crossed the plasmopause, the voltage varied from -5 to +5 V. At 8 R_E the potential reached +20 V (note that in eclipse the potential fell below -3.5 V). Ahmed and Sagalyn [1972], employing spherical electrostatic analyzers on OGO 1, calculated potentials of -3 to -6 V beyond the plasmopause and -11 to -8 V in the plasmasphere. On the same satellite, Taylor et al. [1965], employing an RF spectrometer, estimated -15 V at low altitudes (1500-2700 km) to ~0 V at 30 000 km. As discussed, however, this potential variation may have resulted from the interaction of the exposed positive electrodes on the spacecraft solar cells with the environment. Whipple et al. [1974] reported potentials between 0 and -5.4 V in the plasmasphere on OGO 3 in sunlight. Montgomery et al.

CHAPTER 7

[1973] observed potentials of +100 V in the high latitude magnetotail at 18.5 R_E on Vela 6. (As there were apparently no ion measurements at the time of these estimates, there may be some uncertainty in the method used as a result of possible differential charging [see Whipple, 1976b, or Grard et al., 1977].) During eclipse in the same region, they estimated the potential to be +15 V.

As the satellite potential in eclipse is proportional to the electron temperature, it is not surprising that the most spectacular potential variations have been for geosynchronous

satellites in the plasmashet ($T_E \sim 10$ keV). The best documented and most extensive set of such observations come from the University of California at San Diego (UCSD) particle experiments on the geosynchronous satellites ATS 5 and ATS 6. The large potentials observed by these satellites were first reported and explained by DeForest [1972; 1973], and provided a major impetus to the discipline of spacecraft charging. A typical example of a -10 000 V eclipse charging event in spectrogram format for day 59, 1976, for ATS 6 is presented in Figure 7-2a. In this type

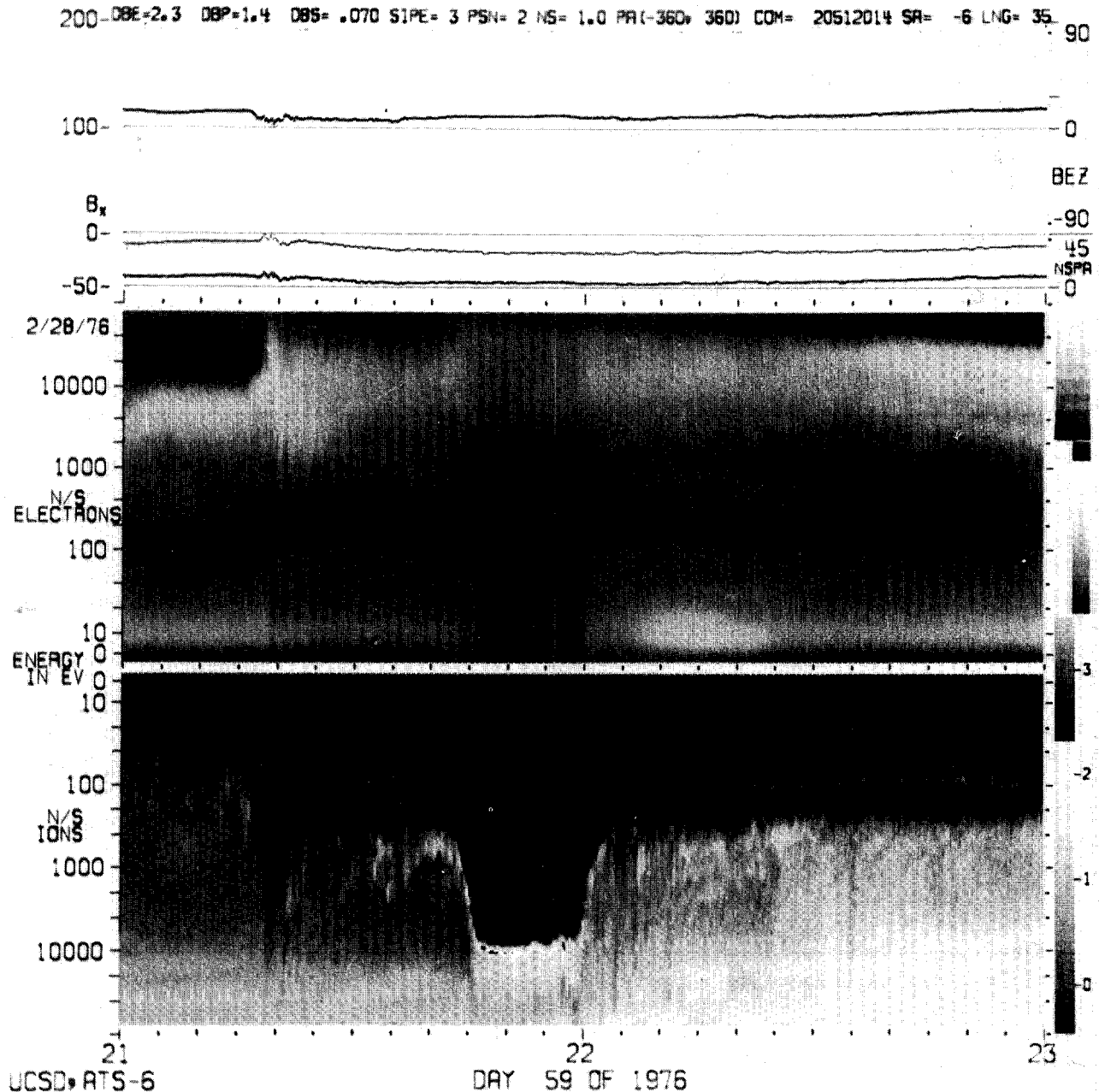


Figure 7-2a. Spectrogram of the UCSD particle detectors on ATS 6 for day 59, 1976 showing a 10-kV charging event between 2140 and 2200 UT.

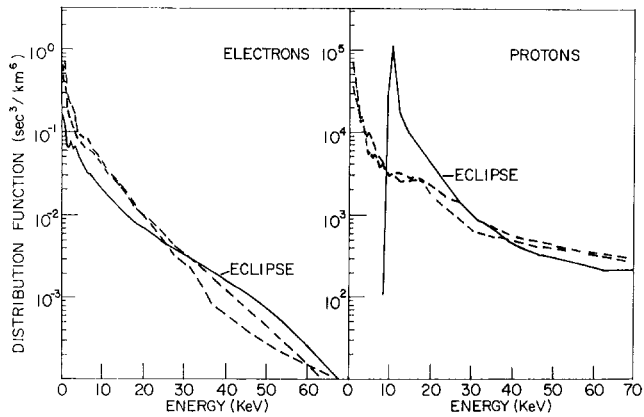


Figure 7-2b. Electron and ion distribution functions versus energy for day 59, 1976. (Dashed lines represent the spectra before and after eclipse; solid lines represent eclipse spectra.)

of plot [DeForest and McIlwain, 1971] the Y axis is particle energy, the X axis is time, and the Z axis (shading) is particle count rates. The figure is interpreted as follows. When the satellite entered eclipse (~2140 UT), the photoelectron flux went to zero shifting the already (100 V) negative potential even more negative. This negative satellite potential V_s accelerated the positive ions as they approached the satellite, adding energy qV_s to each particle. Zero energy positive ions thus appear as a bright band between 2140 and 2200 UT at an energy (10 keV) equal to q times the potential V_s . Electrons, in contrast, were decelerated giving the dropout in the electron spectra between 2140 and 2200 UT. The spectra for before and after eclipse are presented in Figure 7-2b demonstrating this 10 keV shift. Potentials as high as -2000 V [Reasoner et al., 1976] in sunlight and $-20\,000$ V in eclipse have been observed on ATS 6 [S.E. DeForest, 1978, private communication].

Another effect of potential variations, differential charging, is also visible in the ATS 5 and ATS 6 spectrograms. In Figure 7-3, a spectrogram from day 334, 1969, for ATS 5 is presented for the detector looking parallel to the satellite spin axis. Between 0500 and 1100 UT a feathered pattern is visible in the ions and a dropout in the electrons below 750 eV is observed. These patterns are not visible in the detectors looking perpendicular to the satellite spin axis. The explanation [DeForest, 1972; 1973] is that a satellite surface near the detectors has become differentially charged relative to the detectors resulting in a preferential focusing of the ion fluxes and a deficiency in the electron fluxes to the parallel detectors.

The frequency of occurrence of the ATS 5 and ATS 6 charging events in eclipse are presented in Figure 7-4 [Garrett et al., 1978]. The daylight charging events on ATS 6 have been found by Reasoner et al. [1976] (see also Johnson et al. [1978]) to be anticorrelated with encounters with the plasmopause. The level of charging has, however, been found to correlate with K_p (Figure 7-5). To be discussed

later are the ATS 5 and ATS 6 beam experiments [Goldstein and DeForest, 1976; Olsen, 1980; and Purvis and Bartlett, 1980]. These studies presented evidence that while electron emission reduced satellite charging, neutral plasma emission was necessary to achieve zero satellite to space potentials.

Limited observations are available in the solar wind and in the vicinity of the other planets. The Vela satellites typically experienced potentials of $+3$ to $+5$ V in the solar wind [Montgomery et al., 1973]. Whipple and Parker [1969a] computed potentials of $+2.2$ V and $+10$ V for OGO 1 and IMP 2, respectively, in the solar wind. The Voyager spacecraft observed potentials of $+1$ V to $+10$ V [Scudder et al., 1981]. Although preliminary, similar potentials were apparently measured by the Voyager in Jupiter's outer magnetosphere while slightly negative potentials occurred inside the denser, cooler regions of Io's plasma torus [Scudder et al., 1981; see also comments in Grard et al., 1977].

The most complete spacecraft charging measurements are those being made currently by the P78-2 SCATHA satellite (Figure 7-6). P78-2 SCATHA was launched in January of 1979 into a near-synchronous orbit ($5 \times 7 R_E$). The satellite is specifically designed to study spacecraft charging as is evidenced by the extensive list of scientific and engineering instruments (Table 7-1). P78-2 SCATHA has confirmed current ideas concerning the charging process. At the same time, information on the sheaths surrounding a satellite has been obtained. An abbreviated list of observations follows:

1. Arcs were observed under different potential conditions (eclipse, sunlight, beam operations, etc. [Koons, 1980]).
2. The satellite surface potential monitor (SSPM) has determined the response of a number of materials to both natural and artificial charging events [Mizera, 1980]. Sample potentials of over -1000 V have been observed relative to spacecraft ground (see Figure 7-26b).
3. Natural charging events of -1000 V or greater have been observed with one event in excess of -8000 V.

These observations are the first to include simultaneous data on the plasmas, magnetic and electric fields, surface potentials of dielectrics and other surface materials, arcing, and surface contaminants.

The SCATHA data set has been of particular value in defining a "worst case" charging environment for the geosynchronous orbit. In Table 7-2 are listed two "worst case" examples from SCATHA as adapted from Mullen et al. [1981] and Mullen and Gussenhoven [1982]. For comparison with earlier estimates, a "worst case" example from ATS 6 has also been included [Deutsch, 1981]. The plasma moments and single maxwellian temperatures [described in Garrett, 1979] are averaged over all angles while for SCATHA the 2-maxwellian values are for components parallel and perpendicular to the magnetic field. The SCATHA example on Day 114 (24 April 1979, 0650 UT, 2311 MLT)

CHAPTER 7

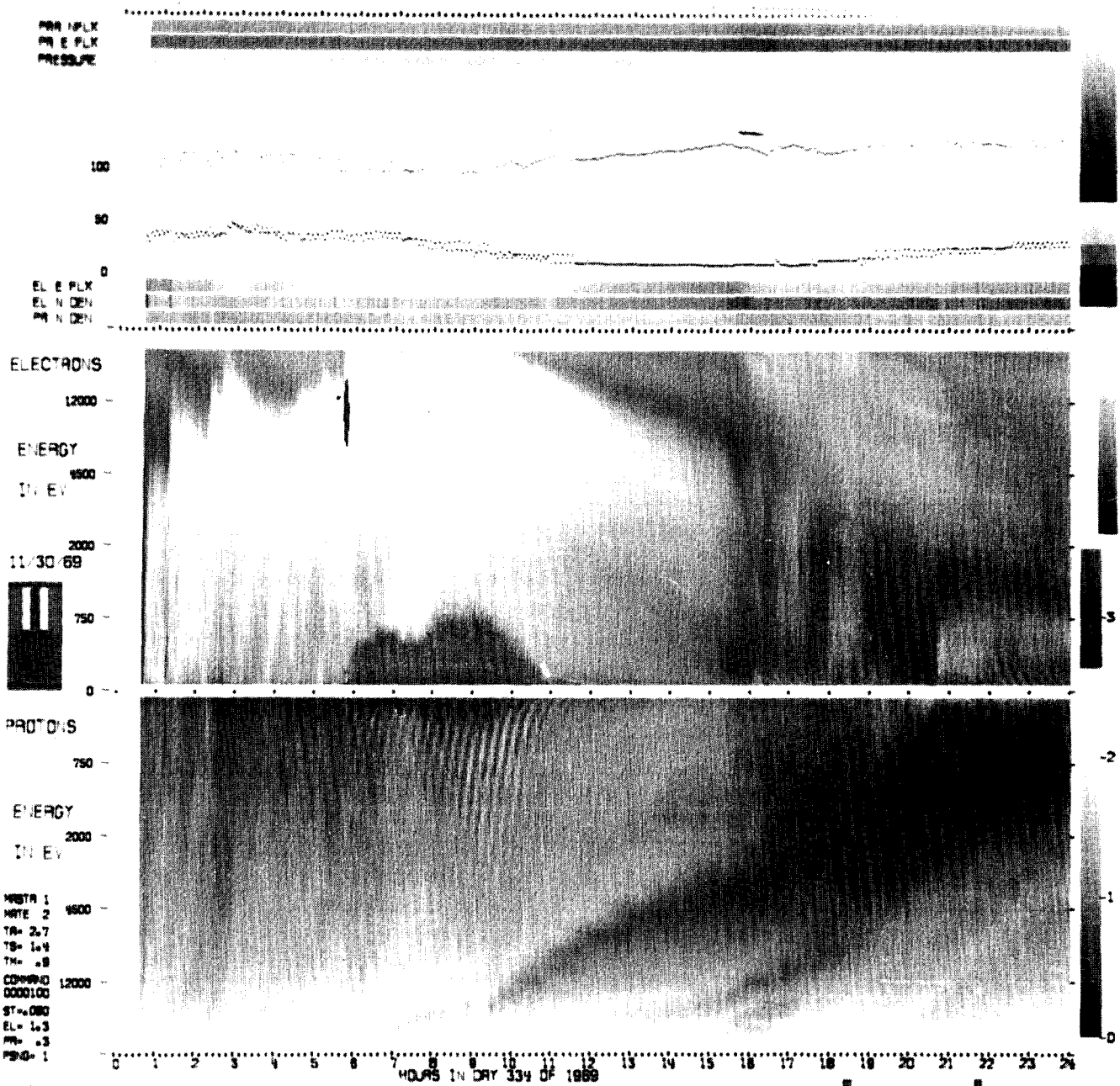


Figure 7-3. Day 334, 1969, spectrogram from ATS 5 [DeForest, 1973]. The feathered pattern in the ions between 0700 and 1100 UT and the corresponding loss of low energy electrons is real and the result of differential charging.

was particularly well documented. For this example, it was found that the vehicle frame potential closely followed the electron current between 33 keV and 335 keV. It is this current that apparently caused the observed high negative vehicle potentials (-340 V in sunlight; estimated to be -16 kV in eclipse). Maximum surface material charging levels for this event were: -3.8 kV on quartz fabric, -6.4 kV on silvered Teflon, and -1.5 kV on aluminized Kapton.

The average ratio of oxygen ions to hydrogen ions was 0.4 during the event.

7.2.3 The Effects of Spacecraft Charging

Aside from direct measurements of spacecraft charging, indirect indicators that reflect the effects of spacecraft charg-

CHARGING OF SPACECRAFT SURFACES

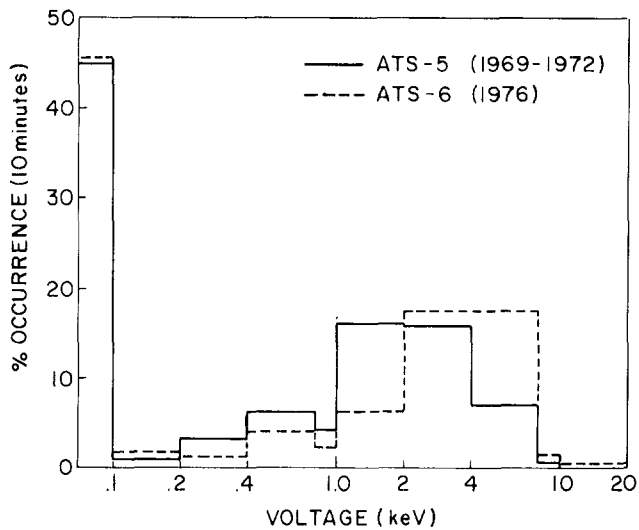


Figure 7-4. Occurrence frequency of ATS 5 (1969-1972) and ATS 6 (1976) eclipse potentials (10-min intervals).

ing also exist. Typical is the plot of satellite operational anomalies as a function of local time at geosynchronous orbit presented in Figure 7-7 [McPherson and Schober, 1976]. The cause of this clustering near local midnight is believed to be spacecraft charging—intense fluxes of energetic electrons associated with injection events are encountered near local midnight which lead to charge buildup and arcing and hence to control circuit upsets and operational anomalies.

Given that differential charging can take place, whether through potential differences on adjoining surfaces or through charge deposition in dielectrics, arcing can occur. Arcing, defined as the rapid (~nanosecond) rearrangement of charge by punchthrough (breakdown from dielectric to substrate), by flashover (propagating subsurface discharge), blowoff (arc to surface), between surfaces, or between surfaces and space, is not well understood. A typical arc discharge pulse [Balmain et al., 1977] is plotted in Figure 7-8. Balmain [1980] finds that surface discharges display characteristics that scale with variations in specimen area according to well

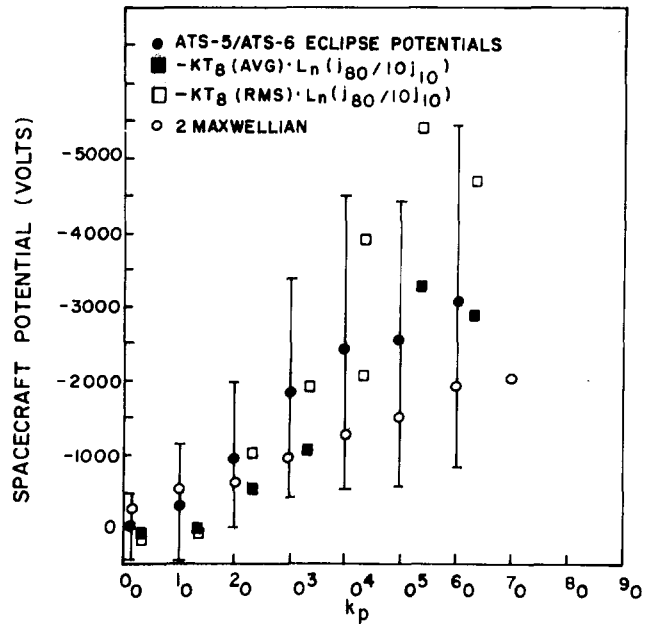


Figure 7-5. Statistical occurrence frequency of observed variations of ATS 5 and ATS 6 eclipse potentials as a function of K_p (solid dots) and various theoretical predictions [Garrett et al., 1979].

defined power laws: peak current scales as the 0.50 power of the area, released charge as 1.00, energy dissipation as 1.50, and pulse duration as 0.53. Although still preliminary, various attempts are also underway to theoretically model these arcing phenomena [Muelenberg, 1976; Beers et al., 1979].

Another result for surface arcs [Stevens, 1980; Nanevicz and Adamo, 1980] in the laboratory is that the breakdown potential on a negative surface varies from -100 V at low earth orbit to $-10\,000$ V at geosynchronous orbit implying that arcing should not be a common occurrence. In Figure 7-9 [Shaw et al., 1976] the arcing rate on a geosynchronous satellite shows a steady increase with the daily geomagnetic index a_p . As arcing is common even at low levels of geomagnetic activity, a discrepancy exists between laboratory

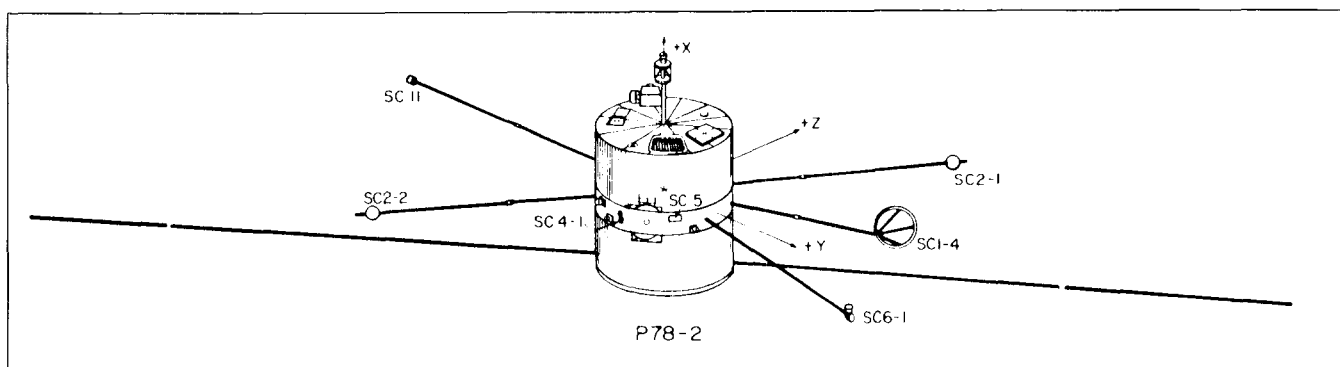


Figure 7-6. The P78-2 SCATHA satellite. The dimensions are approximately 1.3 m wide by 1.5 m high.

CHAPTER 7

Table 7-1. Principal investigators/sponsors for P78-2 SCATHA

Experiment Number	Title	Principal Investigator/ Sponsor	Address
SC1	Engineering Experiments	Dr. H.C. Koons/ USAF/AFSC/SD	The Aerospace Corporation P.O. Box 92957 Los Angeles, CA 90009
SC2	Spacecraft Sheath Electric Fields	Dr. J.F. Fennell/ USAF/AFSC/SD	The Aerospace Corporation P.O. Box 92957 Los Angeles, CA 90009
SC3	High Energy Particle Spectrometer	Dr. J.B. Reagan/ Office of Naval Research	Lockheed Palo Alto Rsch Lab 3251 Hanover Street Palo Alto, CA 94304
SC4	Satellite Electron and Positive Ion Beam System	H.A. Cohen/ USAF/AFSC/AFGL	AFGL/PHG Hanscom AFB, MA 01731
SC5	Rapid Scan Particle	Capt. D. Hardy/ USAF/AFSC/AFGL	AFGL/PHG Hanscom AFB, MA 01731
SC6	Thermal Plasma Analyzer	R.C. Sagalyn/ USAF/AFSC/AFGL	AFGL/PH Hanscom AFB, MA 01731
SC7	Light Ion Mass Spectrometer	Dr. D.L. Reasoner/ Office of Naval Research	NASA Marshall Space Flight Center, Code BS-23 Huntsville, AL 35815
SC8	Energetic Ion Composition Experiment	Dr. R.G. Johnson/ Office of Naval Research	Lockheed Palo Alto Rsch Lab 3251 Hanover Street Palo Alto, CA 94304
SC9	UCSD Charged Particle Experiment	Dr. E.C. Whipple/ Office of Naval Research/USAF/AFSC/SD	University of California B019 Dept. of Physics La Jolla, CA 92093
SC10	Electric Field Detector	Dr. T.L. Aggson/ Office of Naval Research	NASA Goddard Space Flight Center, Code 625 Greenbelt, MD 20771
SC11	Magnetic Field Monitor	Dr. B.G. Ledley/ Office of Naval Research	NASA Goddard Space Flight Center, Code 625 Greenbelt, MD 20771
ML12	Spacecraft Contamination	Dr. D.F. Hall/ USAF/AFSC/AFML	The Aerospace Corporation P.O. Box 92957 Los Angeles, CA 90009
TPM	Transient Pulse Monitor	Dr. J.E. Nanevicz/ USAF/AFSC/SD	SRI Menlo Park, CA

CHARGING OF SPACECRAFT SURFACES

Table 7-2. "Worst" case geosynchronous environments. The moments, TAVG, and TRMS are averaged over all angles. The SCATHA 2-Maxwellian parameters are for fluxes parallel and perpendicular to the magnetic field. ATS 6 2-Maxwellian parameters are averaged over all directions.

SOURCE	DEUTSCH [1981]		MULLEN ET AL. [1981]		MULLEN AND GUSSENHOVEN [1982]	
DATE	DAY 178, 1974 ATS 6		DAY 114, 1979 SCATHA		— SCATHA	
	ELECTRONS	IONS	ELECTRONS	IONS	ELECTRONS	IONS
$\langle ND \rangle$ (cm^{-3})	0.112E + 01	0.245E + 00	0.900E + 00	0.230E + 01	0.300E + 01	0.300E + 01
$\langle J \rangle$ (nA cm^{-2})	0.410E + 00	0.252E - 01	0.187E + 00	0.795E - 02	0.501E + 00	0.159E - 01
$\langle ED \rangle$ (eV cm^{-3})	0.293E + 05	0.104E + 05	0.960E + 04	0.190E + 05	0.240E + 05	0.370E + 05
$\langle EF \rangle$ ($\text{eV cm}^{-2} \text{ s}^{-1} \text{ sr}^{-1}$)	0.264E + 14	0.298E + 12	0.668E + 13	0.430E + 13	0.151E + 14	0.748E + 12
N1 (cm^{-3})	parallel —	0.882E - 02	0.200E + 00	0.160E + 01	0.100E + 01	0.110E + 01
	perpendicular —	—	0.200E + 00	0.110E + 01	0.800E + 00	0.900E + 00
T1 (eV)	parallel —	0.111E + 03	0.400E + 03	0.300E + 03	0.600E + 03	0.400E + 03
	perpendicular —	—	0.400E + 03	0.300E + 03	0.600E + 03	0.300E + 03
N2 (cm^{-3})	parallel 0.122E + 01	0.236E + 00	0.600E + 00	0.600E + 00	0.140E + 01	0.170E + 01
	perpendicular —	—	0.230E + 01	0.130E + 01	0.190E + 01	0.160E + 01
T2 (eV)	parallel 0.160E + 05	0.295E + 05	0.240E + 05	0.260E + 05	0.251E + 05	0.247E + 05
	perpendicular —	—	0.248E + 05	0.282E + 05	0.261E + 05	0.256E + 05
TAVG (eV)	0.160E + 05	0.284E + 05	0.770E + 04	0.550E + 04	0.533E + 04	0.822E + 04
TRMS (eV)	0.161E + 05	0.295E + 05	0.900E + 04	0.140E + 05	0.733E + 04	0.118E + 05

and *in situ* measurements which underscores the need for further analysis.

The effects of arcing are somewhat better understood than the process itself. The current pulse (Figure 7-8) generates an electrical pulse in spacecraft systems either by direct current injection or by induced currents due to the associated electromagnetic wave (see Proceedings of the

IEEE Conference on Nuclear and Space Radiation Effects, 1979). Balmain [1980] and Nanevicz and Adamo [1980] have analyzed the effects of arc discharges on material surfaces. Balmain [1980] gives numerous examples of holes and channels of micron size in dielectric surfaces. Nanevicz and Adamo [1980] find additional, large scale physical damage to solar cells such as fracturing of the cover glass.

Of more immediate concern to the space physics community than arcs, however, are the effects of spacecraft charging on plasma measurements. There are numerous ways that charging can complicate the interpretation of low energy plasma measurements. These can be loosely defined as shifting of the spectra in energy, preferential focusing or exclu-

LOCAL TIME DEPENDENCE OF ANOMALIES

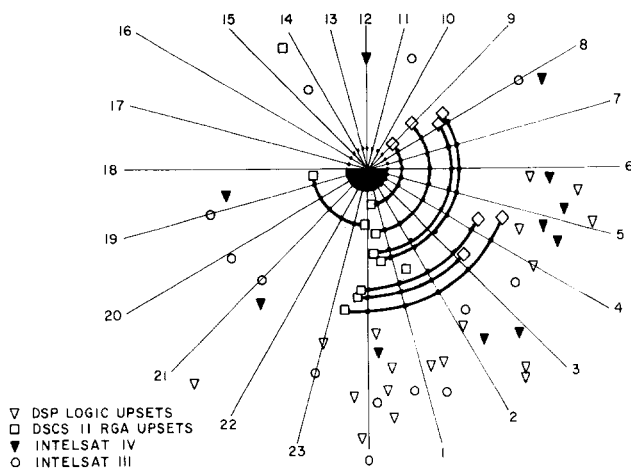


Figure 7-7. Local time plot of satellite operations anomalies; radial distance has no meaning [McPherson and Schober, 1977].

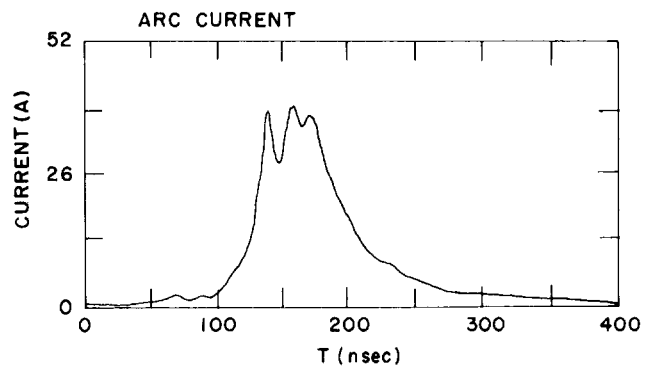


Figure 7-8. Oscilloscope tracing of discharge currents into a conductor supporting a mylar specimen [Balmain et al., 1977].

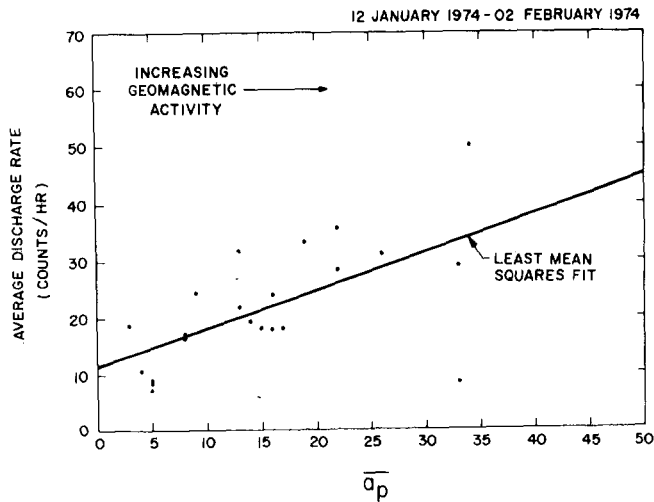


Figure 7-9. Number of arcs per hour as a function of daily a_p for a geosynchronous satellite [Shaw et al., 1976].

sion of particles of a particular energy or direction, and contamination of measurements by secondaries, backscattered electrons, and photoelectrons. Each of these effects is briefly described below.

As described earlier in reference to the ATS 6 observations (Figure 7-2), a potential difference between the vehicle and the ambient plasma can raise or lower the energy of the incoming particles. In the case of differential flux measurements such as the ATS 6 electrostatic analyzers, the shift in energy is easily detected in the attracted species (Figure 7-2). For devices that measure the total current (such as a Langmuir probe) more subtle techniques must be employed which involve intimate knowledge of the current-voltage characteristic.

The most difficult effects to correct are due to particle focusing or exclusion. As demonstrated in Figure 7-3, differential charging of surfaces near a detector can result in focusing or defocusing at specific energies. Just as the geometry of the vehicle can shadow the field of view of a detector, the potential gradients near the detector can distort the particle trajectories. Methods for estimating particle fluxes in the vicinity of such charged surfaces are discussed in Section 7.4.

Secondary electrons, backscattered electrons, and photoelectrons are emitted by spacecraft surfaces. If the vehicle is positively charged, these low energy particles can be reattracted to the vehicle. They constitute an extra and undesirable current source that can confuse ambient electron measurements. Even in the case of negative potentials, differential potentials or space charge potential minima can result in significant secondary and backscattered electrons and photoelectron currents into the detector. This current is easily misinterpreted as a positive potential effect if only electron measurements are available.

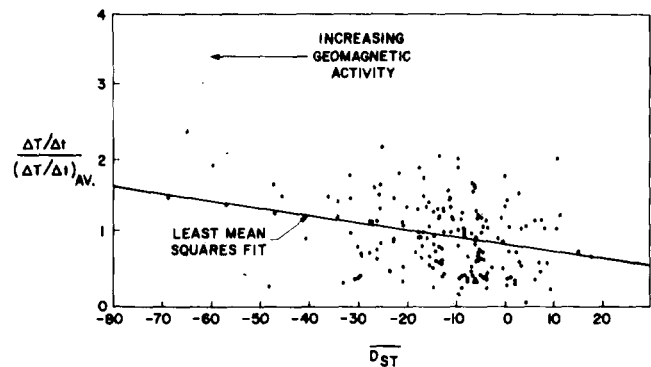


Figure 7-10. Heating rate per day divided by the average heating rate for the entire time period as a function of the daily Dst index [Nanevicz and Adamo, 1980].

Contaminant ions, due to thrusters (ionic or chemical) or outgassing of satellite materials, can be trapped within the satellite sheath and preferentially deposited on negatively charged spacecraft surfaces. Cauffman [1973] (see also Jemiola [1978; 1980]) has estimated that as much as 50 \AA of material can be deposited on charged optical surfaces in as little as 100 days. In Figure 7-10 [Nanevicz and Adamo, 1980] the heating rate of sensors on a geosynchronous satellite apparently rose with geomagnetic activity. This is believed to be due to increased contaminant deposition during periods of geomagnetic activity and, therefore, increased charging (Figure 7-5). Such deposition may also alter secondary emission and photoelectron properties.

Another effect related to charging observed in the laboratory is parasitic power loss. This is anticipated to be important at low orbital altitudes due to interactions between the ambient plasma and exposed high voltage surfaces such as solar cells. McCoy et al. [1980] and Stevens [1980] have estimated this effect both theoretically and by laboratory experiments in large vacuum chambers to result in a 10% power loss for voltages in excess of 5000 V at low earth orbit. They also find that arcing begins at low earth orbit at -100 V and is a significant problem for potentials of -1000 V at geosynchronous orbit. Apparently, the power loss and damage due to such arcing is much more serious on high voltage arrays than parasitic power loss.

7.3 CURRENT MECHANISMS

The spacecraft charging effects reported in the previous section result from current balance, that is, all the various currents of charged particles to and from the satellite surface must balance. Such current balance is valid for a uniform, conducting satellite surface or for a non-conducting surface in the limit of a point. Unless otherwise stated, the former case (for a uniform conducting satellite) will be assumed (if

a non-uniform satellite surface is considered, then the current balance for each isolated surface and the resistive, capacitive, and inductive currents between surfaces must also be considered). The calculation of the satellite surface potential consists of 2 steps. First, the currents to the satellite surface are determined as functions of ambient conditions, satellite geometry, and potential. Second, a satellite potential is found so that current balance is achieved. The calculation of the currents to the satellite surface is very dependent on the fields in the vicinity of the space vehicle. These not only depend on the geometry of the vehicle but also on the sheath or the cloud of charged particles trapped near the satellite. The formulas for calculating the current sources, given the incident particle distribution at each satellite surface, will be described in this section.

7.3.1 Time Scales

In determining the validity of the assumption of current balance, an important issue to consider is the time scales for which it is applicable. Basic electrostatic considerations give order of magnitude estimates of these time scales. As an example, assume the satellite is a conducting sphere of radius r and has a capacitance of C_x ($\propto r$). The time scale τ_{s-s} for the charging of a conducting sphere relative to space in the earth's magnetosphere is then [Katz et al., 1977]

$$\tau_{s-s} \approx \frac{C_x V}{4\pi r^2 J} \approx 2 \times 10^{-3} \text{ s} \quad (7.1)$$

where $r \approx 1 \text{ m}$, V is the satellite potential relative to space ($\sim 1 \text{ kV}$), and J is the ambient flux ($\sim 0.5 \text{ nA cm}^{-2}$).

Unfortunately satellites normally are covered with thermal blankets that consist of thin dielectrics deposited over conducting substrates. The capacitance of a given dielectric area A of thickness s can be estimated by C_D ($\propto A/4\pi s$) so that the time scale τ_D is [Katz et al., 1977]

$$\tau_D \approx \frac{C_D V}{AJ} \approx 1.6 \text{ s} \quad (7.2)$$

where $s \approx 0.1 \text{ cm}$, $V \approx 1 \text{ kV}$, and $J \approx 0.5 \text{ nA cm}^{-2}$.

Other important time scales are the charging time of large, isolated surfaces relative to each other (from seconds to perhaps hours, depending on surface details), the plasma frequency (10^4 – 10^7 Hz), and the gyrofrequency (10^3 – 10^6 Hz for electrons and 10 – 10^3 for H^+); lower values are representative of geosynchronous orbit where $n \sim 1 \text{ cm}^{-3}$ and $B \sim 100 \text{ nT}$, and the higher values for the ionosphere, where $n \sim 10^6 \text{ cm}^{-3}$ and $B \sim 3 \times 10^4 \text{ nT}$. Typically environmental changes take place in minutes or longer, although time scales on the order of the plasma frequency and gyrofrequency are observed. Arcing durations are 10^{-9} – 10^{-8}

s. These time scales imply at least three different ranges for the validity of current balance. Except for the highest frequency ambient electron variations, for plasma frequency variations at low altitudes, and arcing, satellite to space current balance can be realized. Thin dielectrics can respond to typical environmental variations (note this includes ambient variations due to satellite spin modulations, which are usually a few seconds to a minute). Current balance of large surfaces relative to each other may, however, not be achieved (this behavior is illustrated in Figure 7-25b). Thus, current balance is expected to be valid in a number of interesting cases although care must be exercised in the vicinity of the plasma frequency and, in the other extreme, of large isolated dielectric surfaces.

7.3.2 Incident Particle Fluxes

The major natural source of potentials of 10 kV or higher on satellite surfaces is the ambient space plasma. Although space plasma is seldom representable in terms of a single temperature and density, the Maxwell-Boltzmann distribution function is a useful starting point for describing the ambient plasma conditions that generate these large potentials. Given the distribution function f for an isotropic Maxwell-Boltzmann plasma

$$f(v_i) = n_i \left(\frac{m_i}{2\pi k T_i} \right)^{3/2} \exp \left(\frac{-m_i v_i^2}{2k T_i} \right) \quad (7.3)$$

where n_i = number density of species i , m_i = mass of species i , T_i = temperature of species i , v_i = velocity of species i , k = Boltzmann constant, and f = distribution function.

The current flux to a surface in the absence of an electric field is

$$J_{io} = q_i \iiint \mathbf{v}_i \cdot \mathbf{n} f d^3V. \quad (7.4a)$$

Assuming isotropy,

$$J_{io} = \left(\frac{q_i n_i}{2} \right) \left(\frac{2k T_i}{\pi m_i} \right)^{1/2} \quad (7.4b)$$

where J_{io} is the current density per unit area for 0 potential, \mathbf{n} is the unit normal to surface, q_i is the charge on species i , and d^3V is the volume element in velocity space.

As will be shown in Section 7.4, when the effects of the spacecraft potential, sheath or plasma anisotropies, and deviations of the ambient plasma from a Maxwellian distribution are considered, the simple distribution function of Equation (7.3) is no longer valid and the integration of Equation (7.4) becomes difficult. Even so, Equation (7.4)

CHAPTER 7

or a modification of it, is accurate for many practical purposes. Approximate values of T and n for various space plasmas are tabulated in Table 7-3.

7.3.3 Photoelectron Currents

The photoelectron current from a surface is a function of satellite material, solar flux, solar incidence angle, and satellite potential (see review by Lucas, [1973]). In Figure 7-11 adapted from Grard [1973b] are plots of the 4 functions necessary to describe the photoelectron current. In Figure 7-11 the solar flux S is plotted as a function of energy E (or wavelength). The details of the spectrum change with solar activity and can vary greatly if the sunlight reaching the spacecraft is attenuated by the atmosphere [Garrett and DeForest, 1979]. Also shown in Figure 7-11 are the electron yield per photon for normal incidence, W(E), and the total

photoelectron yield H(E) (= W(E)S(E)) as functions of energy for aluminum oxide [Grard, 1973b]. The total current density for zero or negative satellite potential and normal incidence, as derived by Grard, is

$$J_{PHO} = \int_0^{\infty} W(E) S(E) dE = \int_0^{\infty} H(E) dE. \quad (7.5)$$

J_{PHO} for a variety of materials is tabulated in Table 7-4 [Grard, 1973b].

If the satellite is positively charged, the ambient photoelectron current is attracted to the surface. As this return current is a function of potential and geometry, the energy spectrum of the electrons for a given incident monochromatic photon must be known to calculate it accurately. Grard [1973b] has carried out these calculations for several materials and different probe geometries (see also Whipple, [1965]).

Table 7-3. Estimated plasma parameters for various environments. Most values are rough estimates. See appendix.

Region	Altitude	N_0 (cm ⁻³)	Ions	Characteristic Energy (eV)		λ_D (m)		V(km/s)	J_{PH} (nA-cm ⁻²)	Potential (V)**					
				I ⁺	E ⁻	I ⁺	E ⁻			Sunlight			Eclipse		
										1-D	RAM	3-D	1-D	RAM	3-D
<u>Venus</u>	200km	10 ⁵	O ⁺ , O ₂ ⁺	0.05	0.3	0.005	0.01	8	8	-1.2	<u>-1.0</u>	-0.83	-1.8	-1.2	-0.88
	1500km	10 ²	O ⁺	0.2	1	0.33	0.74	8	8	6.0	<u>6.0</u>	2.4	-5.6	<u>-4.4</u>	-2.9
<u>Earth</u>	150km	10 ⁵ D*	O ⁺ , O ₂ ⁺ , NO ⁺	0.1	0.2	0.007	0.01	8	2	-1.1	<u>-0.7</u>	-0.55	—	—	—
		10 ³ N	NO ⁺	0.05	0.1	0.05	0.07	8	2	—	—	—	-0.58	<u>-0.33</u>	-0.37
	1000km	10 ⁴ D	O ⁺	0.3	0.4	0.04	0.05	8	2	-1.3	<u>-1.2</u>	-1.2	—	—	—
		10 ⁴ N	H ⁺	0.2	0.2	0.03	0.03	8	2	—	—	—	-0.75	<u>-0.73</u>	-0.52
	3.5R _E	10 ³	H ⁺	1	1	0.23	0.23	3.7	2	<u>-1.6</u>	-1.6	-1.4	<u>-3.8</u>	-5.2	-2.5
Geosynchronous	5.62R _E	2	H ⁺	5000	2500	370	260	3	2	2.0	1.9	<u>2.0</u>	-8500	-23000	<u>-6500</u>
High Latitude	—	0.1	H ⁺	200	200	330	330	800	2	15.	<u>15.</u>	15.	-750	<u>-490</u>	-500
<u>Jupiter</u>															
Cold Torus	3.5R _J -	50	S ⁺ , O ⁻ , O ⁺	0.5	0.5	0.74	0.74	44	0.08	-0.75	<u>-0.59</u>	-0.72	-2.3	<u>-1.2</u>	-1.6
	5.5R _J	1000		2	1	0.33	0.23	69	0.08	-3.8	<u>-2.2</u>	-3.1	-4.2	<u>-2.3</u>	-3.3
Hot Torus	6.0R _J -	1000	S ⁺ , O ⁺	40	10	1.5	0.74	75	0.08	-37	<u>-34</u>	-33	-39	<u>-34</u>	-33
	8.0R _J -	100		80	20	6.6	3.3	100	0.08	-65	<u>-60</u>	-60	-78	<u>-70</u>	-65
Plasma Sheet	8.0R _J -	12	H ⁺ , S ⁺	50	50	15	15	150	0.08	-110	<u>-110</u>	<u>-94</u>	-190	-170	<u>-130</u>
	15R _J														
Outer Magnetosphere	—	0.01	H ⁺	1000	1000	2300	2300	250	0.08	9.6	9.5	<u>-9.5</u>	-3800	-4400	<u>-2500</u>
<u>Solar Wind</u>															
	0.3AU	50	H ⁺	40	65	6.6	8.5	500	20	4.6	<u>4.9</u>	4.4	-260	<u>-150</u>	-160
	1.0AU	2	H ⁺	10	50	17	37	450	2	7.8	8.0	<u>7.3</u>	-230	-120	<u>-110</u>
	5.2AU	0.2	H ⁺	1	10	17	53	400	0.08	7.4	8.0	<u>6.0</u>	-50	-18	<u>-21</u>

*D = Day, N = Night

**See Appendix for description of computations and captions

Underlined values are "preferred" estimates

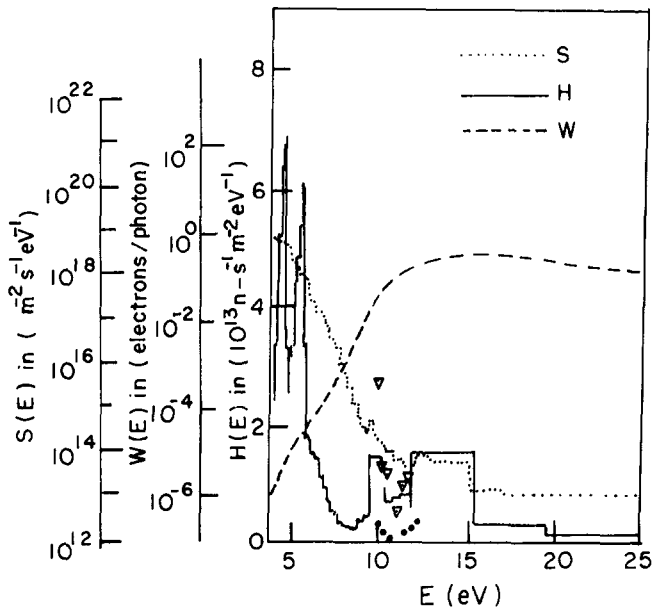


Figure 7-11. Composite plot of $W(E)$, the electron yield per photon; $S(E)$, the solar flux; and their product, $H(E)$, the total photoelectron yield, as function of energy E for aluminum oxide [Grard, 1973].

7.3.4 Backscattered and Secondary Electrons

The impact of ambient electrons and ions on a spacecraft surface generates backscattered and secondary electrons—backscattered and secondary ion fluxes being insignificant. These fluxes, though often neglected in charging calculations can exceed the incident fluxes under some circumstances. Although a clear distinction between secondary and backscattered electrons is not always possible, backscattered electrons are those ambient electrons reflected back from the surface with some loss of energy [Sternglass, 1954] (see also reviews by Dekker [1958], Hachenberg and Brauer [1959], Gibbons [1966], and Lucas [1973].) Secondary

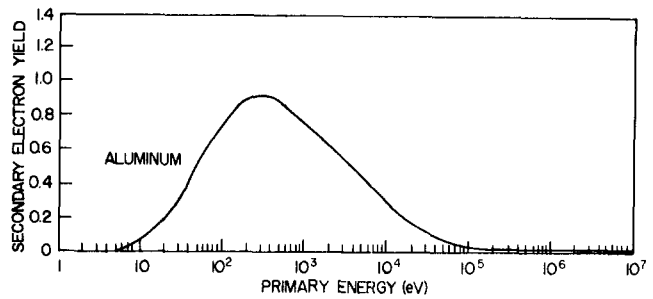


Figure 7-12a. Secondary electron yield δ_E due to incident electrons of energy E impacting on aluminum [Whipple, 1965].

electrons are emitted as a result of energy deposition by incident electrons or ions [Sternglass, 1957; Willis and Skinner, 1973, Chung and Everhart, 1974; Baragiola et al., 1979]. Each of the three has a characteristic emission spectrum.

The equation for the current density due to secondary emission, assuming an isotropic flux and ignoring other angular variations is (see, however, Whipple, [1965]):

$$J_{si} = \frac{2 \pi q_i}{m^2} \int_0^\infty dE' \int_0^\infty g_i(E', E) \delta_i(E) E f_i(E) dE \quad (7.6)$$

where J_{si} = secondary electron flux due to incident species i (usually assumed to be electrons, e^- , or protons, H^+), g_i = emission spectrum of secondary electrons due to incident species i of energy E , δ_i = secondary electron yield due to incident species i of energy E , E' = secondary electron energy, and f_i = distribution function of incident particles at surface.

Typical curves for δ_i for e^- and H^+ impacting on aluminum from Whipple [1965] are plotted in Figure 7-12a and 7-12b (see also Sternglass [1957], Willis and Skinner [1973], Chung and Everhart [1974], and Baragiola et al. [1979]). The function g_i is assumed to be independent of incident energy and incident particle species. The normal-

Table 7-4. Photoelectron emission characteristics of various spacecraft materials.

Material	Work Function (eV)	Photoelectron Saturation Flux ($10^{12} n_e/s\text{-m}^2$)	Saturation Current Density ($\mu\text{ A/m}^2$)
Aluminum Oxide	3.9	260	42
Indium Oxide	4.8	190	30
Gold	4.8	180	29
Stainless Steel	4.4	120	20
Aquadog	4.6	110	18
LiF on Au	4.4	90	15
Vitreous Carbon	4.8	80	13
Graphite	4.7	25	4

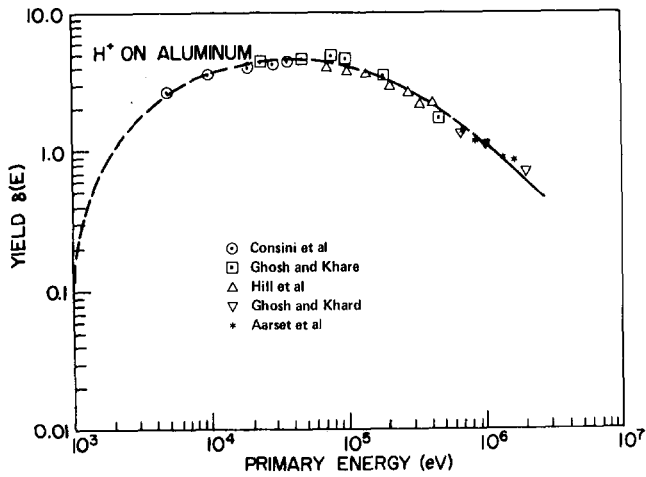


Figure 7-12b. Secondary electron yield δ_1 due to incident ions of energy E impacting on aluminum [Whipple, 1965].

ized curve [Whipple, 1965] for aluminum is plotted in Figure 7-12c.

For backscattered electrons, the current density is given by DeForest [1972]

$$J_{BSE} = \frac{2\pi q_E}{m_E^2} \int_0^\infty dE' \int_{E'}^\infty B(E', E) E f_E(E) dE, \quad (7.7)$$

where

$$B(E', E) = G \left(\frac{E'}{E} \right) \frac{1}{E}$$

and G is the percentage of electrons scattered at fraction E'/E of the incident energy E .

Sternglass [1954] has published experimental measurements of backscatter parameters for different materials. An estimate of G for Al from his data is plotted in Figure 7-13. For negative potentials, the backscatter flux is roughly 20% of the incident flux.

For both secondary and backscattered currents, the ac-

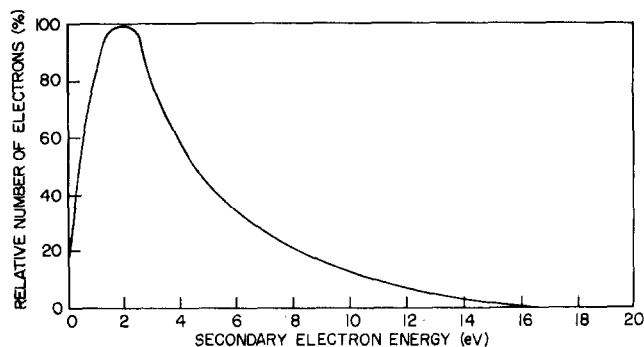


Figure 7-12c. Emission spectrum of secondary electrons due to incident electrons or ions impacting on aluminum [Whipple, 1965].

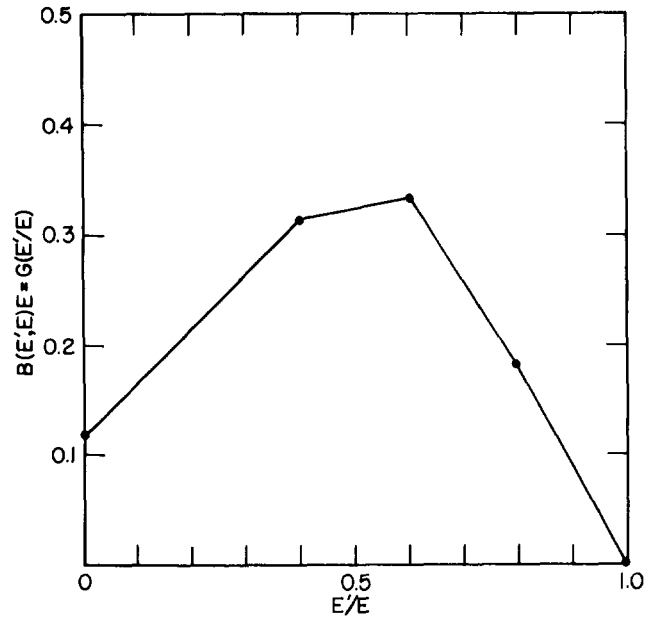


Figure 7-13. Graph of $G(E'/E)$ as a function of (E'/E) where G is approximately the percentage of electrons scattered at a given energy E' as a result of an incident particle of energy E [Sternglass, 1954].

tual values are dependent on angle of incidence which has been ignored in the preceding discussion. Further, the secondary and backscatter properties of actual satellite surfaces which are invariably oxidized or contaminated are not well known. Currently the lack of knowledge in this area is one of the major deficiencies in spacecraft charging theory.

7.3.5 Magnetic Field-Induced Current Distortions

A problem in low earth orbit often encountered by electric field experiments employ long (~ 10 m or longer) antennas or booms is the induced electric field due to the satellite crossing the earth's magnetic field lines. Briefly, a satellite moving relative to a plasma (assumed to have a zero electric field with velocity v_s) will see an electric field E in its rest frame given by

$$E = \frac{v_s \times B}{C} = 10^{-8} (v_s \times B) \text{ V/cm} \quad (7.8)$$

where E is in V/cm, v_s is in cm/s, B is in G, and C is the speed of light.

An earth-orbiting satellite will see a maximum induced $v \times B$ field at low altitudes on the order of ~ 0.3 V/m. The local fields and current flows in the vicinity of the vehicle will be distorted by this effect.

Besides the $v \times B$ current, the magnetic field also induces anisotropies in the particle fluxes. Ambient fluxes, secondaries, beam fluxes, and charged particle wakes are

all controlled to a greater or lesser extent by the magnetic field. Whipple [1965] and Parker and Murphy [1967] have analyzed some of the effects of these magnetic field-induced anisotropies on spacecraft charging (see also reviews by Brundin [1963] and Guverich et al. [1970]) and find that the electron flux can be reduced by as much as a factor of 2, but as a rule these are ignored in spacecraft charging calculations. McCoy et al. [1980] has suggested that this constraint of electrons to field lines may become of real concern for very large structures which are much larger than a gyroradius.

7.3.6 Motion-Induced Effects

In low earth orbit, the velocity of a satellite is 7.5 km/s. Within the plasmasphere, where particle energies are 1 eV or less, the ion thermal velocity is 10 km/s or less. This implies that a plasma wake would be formed around the vehicle. Chang et al. [1979] have estimated that motion-induced effects on the satellite potential due to such a wake are important for ion ram to thermal velocity ratios as low as 0.1. These motion-induced effects would be present even for neutral particles and result in there being large asymmetries in the flow between the leading surfaces of the satellite and the rear for even small objects such as booms. The motion of the satellite can also induce space charge variations in the vicinity of the vehicle [Parker, 1977]. The depletion of electrons and ions in the satellite wake can distort the flow of the particles to the vehicle. A typical observation is presented in Figure 7-14 in terms of the normalized electron fluxes in the wake of the Explorer 31 satellite [Samir and Wrenn, 1969]. Although simple models of this phenomena will be discussed below, reviews by Brundin [1963], Kasha [1969], Liu [1969], and Al'Pert [1976] and papers by Gurevich et al. [1970] and Kunemann [1978] should be consulted for details.

7.3.7 Charge Deposition by Energetic Particles

The deposition of charge in dielectrics by high energy particles is a well known phenomena in nuclear physics (see, for example, Gross and Nablo [1967]; Evdokimov and Tubalov [1974]; and Frederickson [1979]) and has been proposed as a source of satellite charging [Meulenberg, 1976]. As an example [Frederickson, 1980], electrons between 10 keV and 100 keV lose energy at a rate of $R = 10^6$ to 5×10^6 eVg⁻¹cm² depending on energy and the material involved ($R \cdot \rho$, where ρ is the density of the material, gives the energy loss rate per cm). Electrons of 1 MeV will typically penetrate several millimeters into a solid. Fields of the order of M V/mm are necessary to retard such incident fluxes. Fields of this magnitude are more than adequate to cause electrical breakdown in a dielectric. Figure 7-15 is a theoretical plot of the potential in a PCV

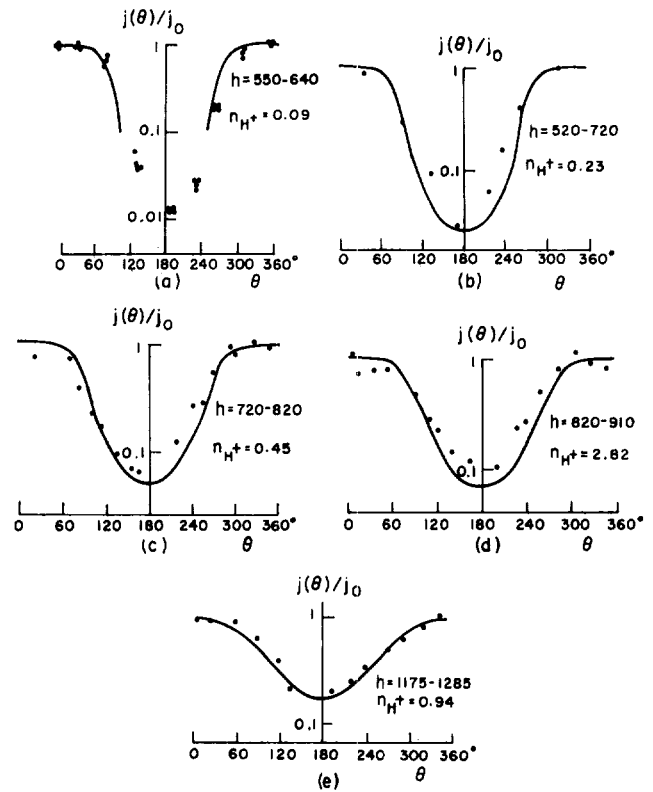


Figure 7-14. Normalized electron current versus angular position of the plasma probe on Explorer 31 [Samir and Wrenn, 1969]; 180° would correspond to the center of the wake (that is, opposite the direction of movement). Also shown are theoretical fits. The altitude h and ambient density n are indicated [Gurevich et al., 1970].

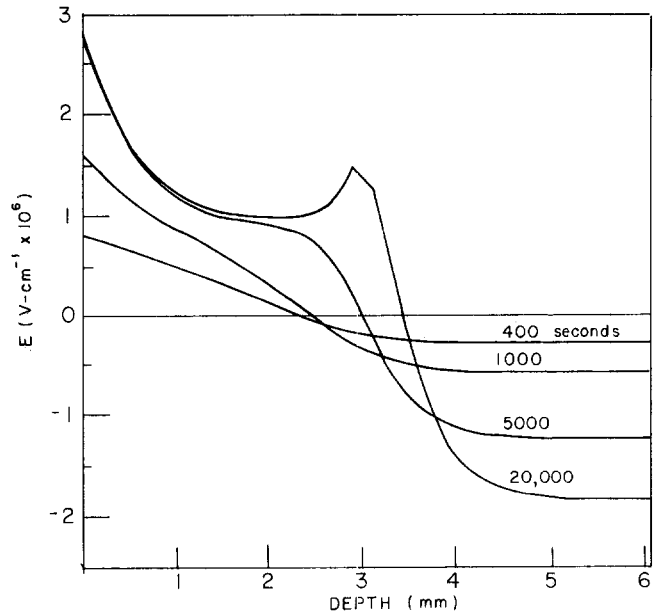


Figure 7-15. The electric field in 6 mm PVC sample as a function of exposure time to a 4.66×10^{-10} A/cm², 1 MeV electron beam [Frederickson, 1980].

CHAPTER 7

sample exposed to 1-MeV electrons as a function of time [Frederickson, 1980].

As satellites in the earth's radiation belts or the hostile environment of Jupiter can experience high dosages of energetic particles, this effect becomes important if long mission lifetimes are desired. Recent evidence [Treadway et al., 1979] indicates that the effects of charging and arcing may be substantially altered by the buildup of charge in dielectrics. As yet, this process has not been included in spacecraft charge modeling. Its inclusion, however, will be critical to a complete understanding of the charging/arcng process.

7.3.8 Artificial Charging Mechanisms

Artificial mechanisms that effect spacecraft charging are numerous and include electron and ion beams and exposed, high potential surfaces such as the junctions between solar cells [Stevens, 1980]. Recently, beam sources have been actively exploited both as probes of the satellite sheath and as a means of controlling the spacecraft potential [Goldstein and DeForest, 1976; Olsen, 1980; Purvis and Bartlett, 1980; Cohen et al., 1979]. Voltages in the KV range and currents between mA and A are typical of these systems [Winkler, 1980]. The Excede 2 test [O'Neil et al., 1978b], in fact, ejected 3 kV electrons at 10 A. An example of a theoretical beam calculation will be given in Section 7.4 as an illustration of the complexities involved in analyzing such experiments.

Parker [1979, 1980], Stevens [1980], McCoy et al. [1980], and Rieff et al. [1980] have carried out calculations of the currents to exposed potential surfaces for large, high voltage structures. They find that a major effect is to induce large voltage gradients in the satellite sheath that must be considered in the proper design and use of such systems. The potentials can lead to multipacting and preferential deposition of ion contaminants. Another possible difficulty associated with very high positive potentials is the "pinhole" effect. As discussed in Kennerud [1974], the insulation on such surfaces can become punctured. Even microscopic holes can result in exceptionally high focusing of electrons—in some cases the pinhole can completely defeat the insulation.

Finally, a number of experiments have been conducted in vacuum chambers. Currently, the most extensive programs are those at NASA Johnson [McCoy et al., 1980] and NASA Lewis [Stevens, 1980; Purvis et al., 1977; and their colleagues]. The NASA Johnson chamber tests have involved testing of high potential surfaces and of rocket beam sources prior to flight [Konradi, private communication, 1980] in an environment resembling the ionosphere. As discussed in Bernstein et al. [1978; 1979], these latter tests have concentrated on the analysis of the so-called "beam-plasma discharge" (BPD) in electron beam experiments. They have found that the electron beam at a critical current transitions from one well defined by single particle dynamics

to a much larger beam spread marked by an increase in the local plasma density. The critical current I_C when this occurs is proportional to the beam energy, V_B , such that $I_C \propto V_B^{3/2}$, an equation resembling Equation (7.14). The NASA Lewis studies are part of a coordinated effort to validate the NAS-CAP code (see Section 7.4.6) and have included testing of the P78-2 SCATHA experiments [Stevens et al., 1980a].

7.4 SPACECRAFT CHARGING THEORY

The basic equation expressing current balance for a given surface in an equilibrium situation is, in terms of the current:

$$I_E(V) - [I_I(V) + I_{SE}(V) + I_{SI}(V) + I_{BSE}(V) + I_{PH}(V) + I_B(V)] = I_T \quad (7.9)$$

where V = satellite potential, I_E = incident electron current on satellite surface, I_I = incident ion current on satellite surface, I_{SE} = secondary electron current due to I_E , I_{SI} = secondary electron current due to I_I , I_{BSE} = backscattered electrons due to I_E , I_{PH} = photoelectron current, I_B = active current sources such as charged particle beams or ion thrusters, and I_T = total current to satellite (at equilibrium, $I_T = 0$).

In this section methods of solving Equation (7.9) for V so that $I_T = 0$ will be described. The basic problem is the solution of Equation (7.9) subject to the constraints of Poisson's equation:

$$\nabla^2 V = 4 \pi q(n_s + n_E - n_I) \quad (7.10)$$

and the time-independent collisionless Boltzmann (or Vlasov) equation:

$$\mathbf{v} \cdot \nabla f_i - \frac{q_i}{m_i} \nabla V(\mathbf{r}) \cdot \nabla_v f_i = 0, \quad (7.11)$$

where n_E = local electron density, n_I = local ion density, n_s = surface-emitted electron density, ∇ , and ∇_v = gradient operators with respect to position and velocity space respectively.

7.4.1 Analytic Probe Theory General Considerations

The most important concept in probe theory is that of the Debye length λ_D , the distance over which a probe or satellite significantly perturbs the ambient medium. (Note that this is only one definition of the satellite sheath. The sheath thickness is not only dependent on satellite potential and charge, but through the so-called "presheath", influences the plasma up to the order of the satellite radius

CHARGING OF SPACECRAFT SURFACES

[Parker, 1980]. More precisely, electrons and ions form a cloud around any charged surface that is a function of the particles' energies and densities and the potential on the surface. As an illustration, the solution to Poisson's equation for spherical symmetry is

$$V(r) = q \frac{e^{-r/\lambda_D}}{r} \quad (7.12)$$

where $\lambda_D = (KT/4\pi q^2 n_0)^{1/2}$ and $n_0 =$ ambient charge density. This is the classical Debye length for the assumption of "linearized space charge." The "linearized space charge" approximation can be extended to spherical and other multi-dimensional geometries; an analytical fit for the spherical case is discussed by Parker [1980]. Values for λ_D are listed in Table 7-3.

The terminology "thick" sheath and "thin" sheath derives from the assumption that the region over which the satellite affects the ambient plasma or is screened from the ambient plasma is either larger or smaller than the characteristic dimensions of the spacecraft. Usually this reduces to determining whether λ_D is long (thick sheath) or short (thin sheath) compared to the spacecraft radius. From Table 7-3, for a 1 m radius spacecraft with no exposed potential surfaces in low earth orbit, the term thin sheath is appropriate. For geosynchronous orbit, unless the satellite is 10 m or larger, the thick sheath approximation is appropriate. If active surfaces (that is, exposed potentials driven by the satellite systems) or a substantial photoelectron population are present, these limiting criteria will change, but even so for most satellite studies they are very useful (Opik [1965] has carefully considered this issue of the appropriate screening criteria for the general case of an arbitrary central force).

As a first example, consider a large structure such that the characteristic scale of the sheath is significantly smaller than r_s , the radius of the surface (the thin sheath assumption). Assuming at the surface ($X = r_s$) the potential is V_0 and that the surface is nearly planar relative to the sheath dimensions, at distance $Y (= X - r_s)$ from the surface (only the attracted species is considered)

$$\text{Poisson's Equation} \quad \frac{d^2 V(Y)}{dY^2} \approx -4\pi q n(Y) \quad (7.13a)$$

Current continuity

$$J = q n(Y) v(Y) = \text{constant} \quad (7.13b)$$

The particles are assumed to have $E = 0$ in the ambient space:

Energy conservation

$$\frac{1}{2} m v(Y)^2 + q V(Y) = 0. \quad (7.13c)$$

In order to solve these equations, it is assumed that V and $dV(Y)/dY$ are 0 at some distance $Y = S$ which determines the sheath thickness (called the "space-charge limited" assumption). The solution becomes

$$J = \frac{1}{9\pi} \left(\frac{2q}{m}\right)^{1/2} \frac{V_0^{3/2}}{S^2} \quad (7.14)$$

This is the "space-charge limited diode model" solution or Child-Langmuir model for a plane. If J is replaced by $J_0 = K^* q n_0 (kT/m)^{1/2}$ (where $(2\pi)^{-1/2} < K^* < 1$, the lower limit corresponds to Equation (7.4b); the upper limit is for a monoenergetic flow of energy $E \equiv 1/2 kT$) then the sheath thickness can be estimated:

$$S = \frac{1}{3} \left(\frac{2}{qKT}\right)^{1/4} (V_0)^{3/4} \left(\frac{1}{\pi n_0}\right)^{1/2} \left(\frac{1}{K^*}\right)^{1/2}. \quad (7.15)$$

This sheath thickness determines the region over which charge is collected and is important in determining the maximum current that can flow to a probe for a given V .

Although seldom utilized in spacecraft charging calculations, a form of Equation (7.14) was employed by Beard and Johnson [1961] to obtain the potential to which a vehicle can be charged by an electron emitter in the ionosphere. This calculation placed an upper limit on the current that could be drawn at a given potential ignoring magnetic field shielding effects. When included [Parker and Murphy, 1967], the maximum current was reduced by as much as a factor of 10. Linson [1969], including turbulence, found values between these limits, however. These studies imply that a 1 m sphere emitting a 0.5A electron beam at shuttle altitudes would have a potential of 10^4 – 10^6 V, depending on the magnetic field [Liemohn, 1977], thereby seriously inhibiting a 10–100 keV beam. Recently, Parker [1980] (see also Kennerud [1974], McCoy et al. [1980], and Parks and Katz [1981]), in order to estimate the sheaths around large space structures, have developed an analytic expansion for the thin sheath approximation to a sphere. He has investigated the applicability of this estimate of the sheath to extremely high applied potentials in the ionosphere by comparing it to the results of a self-consistent numerical calculation (see Section 7.4.2). Although his rigorous computations (for a Debye length to satellite radius ratio of 1 to 100) deviate at low potential values ($qV/kT \lesssim 10$) from the space charge limited model, the results approach each other for very high potentials ($qV/kT \sim 400,000$).

The preceding theory concerning the thin sheath assumes that sheath effects dominate the current flow to the satellite. This places emphasis on Poisson's equation and the space charge around the satellite. In the opposite extreme, the sheath and space charge are ignored so that, to first order, Laplace's equation holds. In practical terms this translates into the assumption that $\lambda_D \gg r_s$. For spherical symmetry, conservation of energy and angular momentum imply that

CHAPTER 7

for an attracted particle approaching the satellite from infinity

$$\frac{1}{2} m v_o^2 = \frac{1}{2} m v(r_s)^2 + q V(r_s) \quad (7.16a)$$

$$m R_I v_o = m r_s v(r_s) \quad (7.16b)$$

where v_o is the velocity in ambient medium, R is the impact parameter, and R_I is the R for a grazing trajectory for a vehicle of radius r_s .

Solving for the impact parameter R_I (only particles having $R < R_I$ will reach r_s):

$$R_I^2 = r_s^2 \left(1 - \frac{2qV(r_s)}{mv_o^2} \right) \quad (7.17)$$

$(R_I - r_s)$ is equivalent to the sheath thickness S defined for a thin sheath as it also is the size of the region from which particles can be drawn.

The total current density striking the satellite surface for a monoenergetic beam is

$$J(V) = \frac{I}{4\pi r_s^2} = J_o \left(1 - \frac{2qV(r_s)}{mv_o^2} \right) \quad (7.18)$$

where I is the total current to spherical satellite equal to the ambient current that would pass through an area $4\pi R_I^2$ and J_o is the ambient current density outside the sheath equal to $I/4\pi R_I^2$. This is the so-called "thick sheath, orbit-limited" current relation.

The thick sheath results are readily extended to more complex distributions. For most spacecraft charging problems, Boltzmann's equation [Equation (7.11)] in the absence of collisions reduces to Liouville's theorem. For a complex distribution function, F , Liouville's theorem states that:

$$F(\mathbf{v}) = F'(\mathbf{v}') \quad (7.19)$$

where F' and \mathbf{v}' are the distribution function and velocity at the surface of the spacecraft. F and \mathbf{v} are the ambient distribution and velocity at the end of the particle trajectory connected to the satellite surface where F' and \mathbf{v}' are measured. Prokopenko and Laframboise [1977, 1980] have derived (based on Equation (7.19)), in more general terms the current density to a sphere, infinite cylinder, and infinite plane (that is, three-, two-, and one-dimensions) for a Maxwell-Boltzmann distribution for the orbit-limited solution. Their results (see original derivation in Mott-Smith and Langmuir [1926]) for the attracted species are

$$J_i = J_{i0} \cdot \begin{cases} (1 + Q_{is}) & \text{Sphere} \\ [2(Q_{is}/\pi)^{1/2} + e^{Q_{is}} \operatorname{erfc}(Q_{is}^{1/2})] & \text{Cylinder} \\ (1) & \text{Plane} \end{cases} \quad (7.20)$$

and for the repelled species $J_i = J_{i0} e^{Q_{is}}$ where

$$Q_{is} = \pm \frac{qV}{kT_i} \quad (+ \text{ for electrons, } - \text{ for ions}) \quad (7.21)$$

The current-voltage characteristics implied by Equations (7.20) and (7.21) for the three geometries are plotted in Figure 7-16. Several important conclusions can be drawn from Equations (7.20) and (7.21) and Figure 7-16. First Prokopenko and Laframboise's results for a sphere are identical to Equation (7.18) (with $1/2 mv_o^2$ replaced by kT_i) for

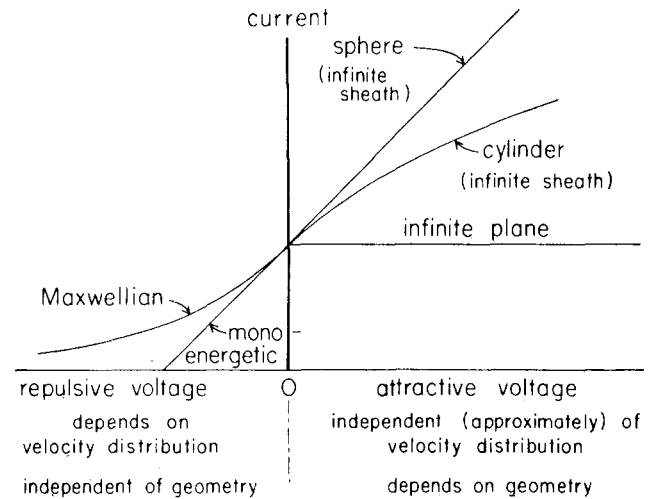


Figure 7-16. Qualitative behavior of Equations (7.20) and (7.21) for a Langmuir probe [Parker and Whipple, 1967]. (Reprinted with permission of Academic Press © 1967)

a thick sheath. It should also be readily apparent that the planar solution is conceptually equivalent to a thin sheath. Thus, Equation (7.20) additionally gives a qualitative picture of how the probe characteristics change as the ratio of the Debye length to satellite radius is varied from small values (thin sheath or planar) to large values (thick sheath or spherical). This was done explicitly by Whipple et al. [1974] and Whipple [1977] for the ratio of the Debye length to satellite radius and is closely related to the parametrization method of Cauffman and Maynard [1974].

7.4.2. Analytic Probe Theory Thick Sheath Models

At this point a complete analytic theory for the case of a thick sheath, spherical probe has been developed. Substituting into Equation (7.10) and assuming that the secondary and backscatter terms can be parametrized, for an ambient Maxwellian plasma

$$\begin{aligned}
 & A_E \cdot J_{EO} \cdot [1 - SE(V, T_E, n_E) - BSE(V, T_E, n_E)] \\
 & \cdot \exp(qV/kT_E) \\
 - & A_I \cdot J_{IO} \cdot [1 + SI(V, T_I, n_I)] \cdot \left(1 - \frac{qV}{kT_I}\right) \quad (7.22) \\
 - & A_{PH} \cdot J_{PHO} \cdot f(X_m) = I_T = 0 \quad V < 0
 \end{aligned}$$

where

J_{EO} = ambient electron current density [Equation (7.4)]

J_{IO} = ambient ion current density [Equation (7.4)]

A_E = electron collection area ($4 \pi r_s^2$ for a sphere)

A_I = ion collection area ($4 \pi r_s^2$ for a sphere)

A_{PH} = photoelectron emission area (πr_s^2 for a sphere)

SE, SI, BSE = parametrization functions for secondary emission due to electrons and ions and backscatter

J_{PHO} = saturation photoelectron flux (Table 7-4)

$f(X_m)$ = percent of attenuated solar flux as a function of altitude X_m of center of sun above the surface of the earth as seen by satellite.

Equation (7.22) is appropriate for a small (<10 m), uniformly conducting satellite at geosynchronous orbit in the absence of magnetic field effects. To solve the equation, V is varied until $I_T = 0$. A number of examples of this procedure, assuming $SI = SE = BSE = 0$, are tabulated in Table 7-3 for various plasma regions.

If it is assumed that SI, SE, and BSE are constants (that is, ~ 3 , ~ 0.4 , and ~ 0.2 for A1), then Equation (7.2) predicts [Garrett and Rubin, 1978] that in eclipse, the potential between the satellite and space is

$$V \approx -T_E \quad (7.23)$$

The satellite to space potentials observed by UCSD electrostatic detectors for twenty-one ATS 5 and four ATS 6 eclipses are plotted in Figure 7-17 versus the electron temperature. As the geosynchronous plasma is not necessarily Maxwellian, two different "temperatures," T_o (AVG) ($= 2/3 \cdot \text{energy density/number density}$) and T_o (RMS) ($= 1/2 \cdot \text{energy flux/number flux}$), are presented (these would be equal if the plasma was actually Maxwellian). The agreement is good considering that the range of potentials is between -300 V and $-10\,000$ V. The existence of a

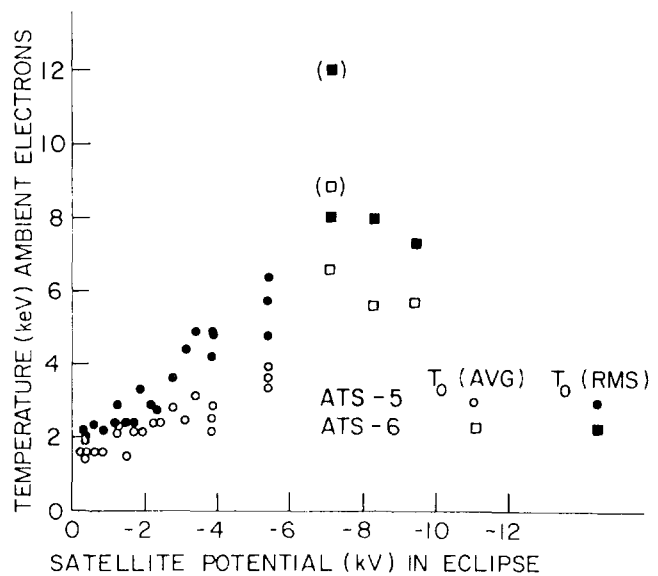


Figure 7-17. Observed temperature of ambient electrons versus satellite potential in eclipse. T_o (AVG) is two thirds of energy density/number density; T_o (RMS) is one half of energy flux/number flux.

threshold temperature below which charging does not occur is real and is due to the fact that at an intermediate energy (usually a few hundred eV), the secondary yield is greater than 1 [Rubin et al., 1978]. The electron temperature must be several times greater than this threshold energy before charge buildup occurs.

The agreement can be significantly improved for Figure 7-17 if the actual ambient spectra are utilized in the integration of Equations (7.4), (7.6), and (7.7) instead of a Maxwellian in computing the currents. This method of using the actual particle spectra to estimate the currents has been extensively employed by DeForest [1972], Knott [1972], Garrett and DeForest [1979], and Prokopenko and Laframboise [1977, 1980] in the calculation of satellite to space potentials for geosynchronous spacecraft. The potentials of Figure 7-17 are recalculated in this manner and plotted in Figure 7-18a [Garrett and DeForest, 1979]. Results are presented both for particle spectra immediately before entry or immediately after exit from eclipse ("sunlit") and for eclipse ("eclipsed"); differences are attributed to the digitization of the spectra. As the exact secondary response of the satellite surface was not known, SE, SI, and BSE were assumed to follow the A1 curves of Figures 7-12 and 7-13. Their absolute amplitudes were then varied until the observations were fit in a least squares sense [Garrett and DeForest, 1979].

Given the validity of the calibration method, the effects of a varying photoelectron flux on the satellite to space potential can be studied during eclipse passage. If the satellite position is known, the photon flux reaching the satellite can be calculated from first principles [Garrett and Forbes,

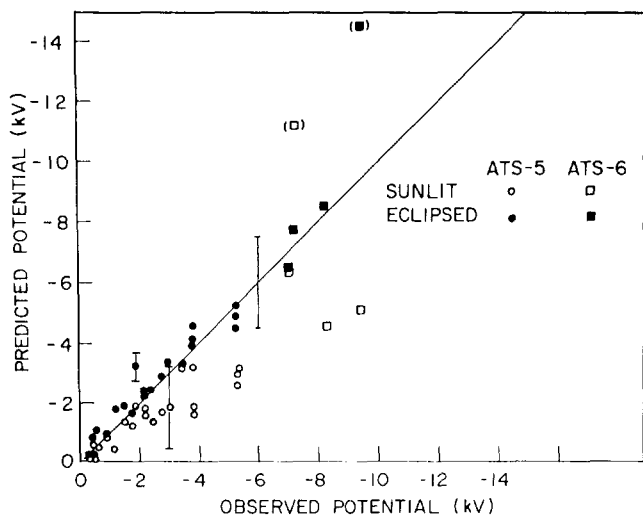


Figure 7-18a. Predicted and observed potentials in eclipse for ATS 5 and ATS 6. Solid symbols are for calculations using the spectra in eclipse. Open symbols are for calculations using the spectra measured in sunlight.

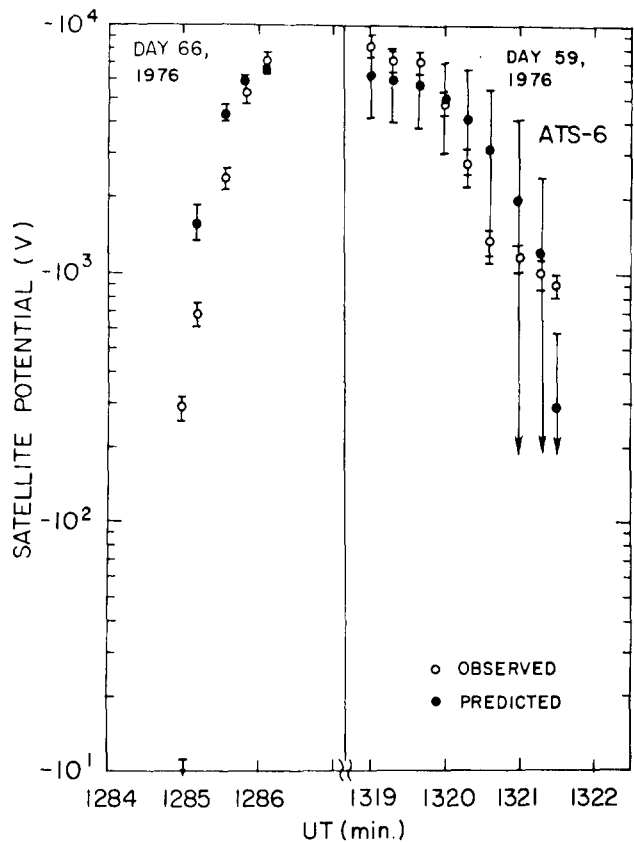


Figure 7-18b. Observed and predicted potentials for the entry into eclipse of ATS 6 on day 66, 1966, and for eclipse exit on day 59, 1976.

1981]. If the satellite surface materials were known, then the photoelectron current, $J_{PHO} \cdot f(X_m)$, could also be calculated from first principles. Although the exact surface response is in actuality not known, adequate approximations can be derived [Garrett and DeForest, 1979; Garrett and Forbes, 1981]. J_{PHO} in Equation (7.22) is then varied to fit observations. Estimates of the varying potential on ATS 6 during eclipse entry and exit by this technique are compared with actual observations in Figure 7-18b [Garrett and DeForest, 1979]. This eclipse model has proven valuable in estimating photoelectron flux and potential variations for ATS 5, ATS 6, Injun 5, and P78-2 SCATHA.

The results of Prokopenko and Laframboise [1977, 1980], using the spectra suggested by Knott [1972], are particularly important because they established the existence of multiple roots for Equation (7.22) (see also Sanders and Inouye [1979]). Multiple roots imply that a satellite can undergo rapid voltage variations in response to small environmental perturbations and that adjacent surfaces can come to radically different potentials for the same conditions. To obtain their result, they solved an equation equivalent to Equation (7.22) (that is, local current balance) for the spherical, the cylindrical, and planar assumptions of Equations (7.20) and (7.21) and for eclipse conditions. They found that the potential is markedly increased for a planar probe relative to a spherical probe.

7.4.3 Analytical Probe Theory Thin Sheath and Related Models

Analytic probe theory can also be utilized to estimate satellite to space potentials in the 250–700 km range. As discussed in Brundin [1963], in the absence of magnetic forces, photoelectrons, and secondaries, Equation (7.9) reduces to

$$A_E \cdot J_{EO} \cdot C_E \cdot e^{qV/kT_E} - A_I \cdot J_{IR} \cdot C_I = 0 \quad (V < 0) \quad (7.24)$$

where

J_{EO} = ambient electron current density (Equation (7.4)),

J_{IR} = ion ram current density (ignoring ion thermal velocity)

$$= q_I n_I v_s,$$

v_s = satellite velocity,

A_E = electron collection area ($4 \pi r_s^2$ for a sphere),

A_I = ion collection area (πr_s^2 for a sphere),

r_s = satellite radius

CHARGING OF SPACECRAFT SURFACES

C_E = electron shielding factor (= 1, no electron wake assumed; $\approx 1/2$, wake on rear half),

C_i = ion shielding factor {(= 1, complete shielding of ambient ions or thin sheath;
 $= \left(1 - \frac{2qV}{m_i v_s^2}\right)$, no shielding or thick sheath,
 (Equation (7.18)).

Samir [1973] and Samir et al. [1979b], assuming no electron wake and no ion shielding (note that this is a thick sheath assumption which is usually inappropriate in this region), have compared the predictions of Equation (7.24) with observations. In spite of the simplicity of Equation (7.24) and the assumption of a thick sheath, they predict the satellite to space eclipse potential (typically $\sim -0.75V$) for a large range of ambient conditions to a factor of 2.5 or better.

A simple approximation for estimating the current to an isolated point on a planar satellite surface in the ionosphere as a function of the surface normal relative to the velocity vector is that of Whipple [1959] and Bourdeau et al. [1961] (see also Tsien [1946] and Chang et al. [1979]):

$$I_i = \alpha q n_i A_i \left[v_s \cos \theta (1/2 + 1/2 \operatorname{erf}(x)) + \frac{ae^{-x^2}}{2\sqrt{\pi}} \right] \quad (7.25)$$

where

$$x = \frac{v_s \cos \theta}{a} - \left(\frac{qV}{kT_i} \right)^{1/2},$$

θ = angle between sensor normal and velocity vector,

A_i = collection area,

α = grid transparency function,

a = most probable ion thermal velocity.

This equation, the so-called "planar approximation", is good for short Debye lengths but becomes inaccurate for long Debye lengths [Parker and Whipple, 1970] and more complicated orbital trajectory calculations must be carried out. Even so, Bourdeau et al. [1961] found it to be a good approximation to the ion current relative to the velocity vector measured by the ion current planar probe on Explorer 8 (425–2300 km altitude). Their results for $V = 0$ are plotted in Figure 7-19 (note that there is some question as to the best value for a , see Bourdeau et al. [1961]).

A simple analytic theory closely related to thin sheath probe methodology and capable, within limits, of explaining the satellite wake structure in the ionosphere has also been developed. It (see reviews in Gurevich et al. [1970] and Al'pert [1976]) is based on the thin sheath assumption,

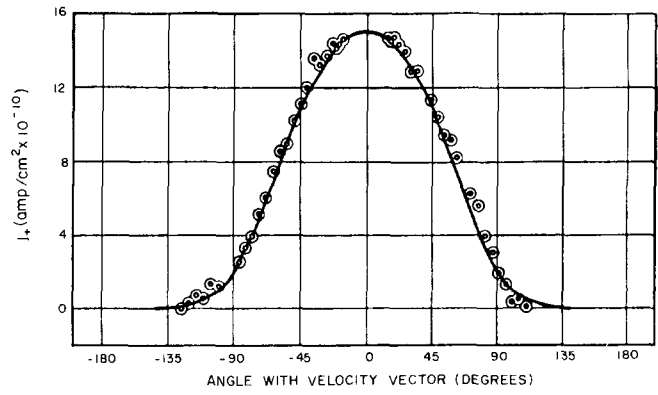


Figure 7-19. Variations in the positive ion current density with angle relative to the satellite velocity vector. The data and figure are from Bourdeau et al. [1961]. The fitted line is given by Equation (7.29) with a assumed to be 3.6 km/s; the satellite potential is assumed to be 0.

$r_s \gg \lambda_D$, the Debye length in the ionosphere being much smaller than the satellite's characteristic dimensions. This allows the neglect of the effects of the satellite potential except very close to the satellite surface. The left hand side of Equation (7.10) can then be ignored, so that it becomes:

$$n_E - n_i \approx 0 \quad (7.10^*)$$

This is the so-called "quasi-neutrality" assumption [for example, Gurevich et al., 1966, 1968, 1973; Grebowski and Fischer, 1975; Gurevich and Dimant, 1975; Gurevich and Pitavetskii, 1975]. Equation (7.11) for the ions can be reduced by making use of the "hypersonic" character of the motion of a body in the ionosphere (that is, M , the square root of the ratio of the ion kinetic energy to electron thermal energy, is much greater than 1). First, this implies that the gradient of the potential *perpendicular* to the flow direction is much greater than the gradient *along* the flow direction so that this latter term can be ignored. Second, the thermal velocity of the ions in the direction *along* the flow direction can be neglected relative to the satellite velocity v_s in the ionosphere. Based on these assumptions, Equation (7.11) for ions can be rewritten as

$$v_s \frac{\partial f_i}{\partial z} + \mathbf{v}_\perp \cdot \frac{\partial f_i}{\partial \mathbf{r}_\perp} - \frac{q}{m_i} \frac{\partial V}{\partial \mathbf{r}_\perp} \cdot \frac{\partial f_i}{\partial \mathbf{v}_\perp} = 0 \quad (7.11^*)$$

where \mathbf{r}_\perp and \mathbf{v}_\perp correspond to components normal to the direction of motion and z is in the \mathbf{v}_s direction.

For the electrons, a Boltzmann distribution ($n_E = n_{E0} \cdot \exp(qV/KT_E)$) is usually assumed. The resulting system of equations for the ions does not contain the ion thermal velocity along the direction of motion and can be put into a dimensionless, self-similar form [Al'pert et al., 1965; Gurevich et al., 1970] that resembles classical hypersonic aerodynamic equations. Depending on the char-

CHAPTER 7

acteristics of the assumed plasma conditions, the wake variations for a number of simple geometries can be analytically solved. These range from the extreme assumption of a true neutral flow as reviewed in Gurevich et al. [1970] and Al'pert [1976]—charged particle variations in the wake mirroring the neutral variations—to plasma flows around infinite half-planes, wedges, plates, cylinders, and discs. The predictions for one such analytic solution [Gurevich et al., 1970] are compared with Explorer 31 observations in Figure 7-14 from Samir and Wrenn [1969] for various distances r/r_s from the satellite. The theory is not considered reliable at angles greater than $\sim 120^\circ$ as the electron density can differ greatly from the ion density in this region of maximum rarefaction [Gurevich et al., 1970].

Although severe constraints (primarily $r_s \gg \lambda_D$ and neglect of the ion thermal velocity) have been placed on the realm of applicability of this “hypersonic,” quasi-neutral theory, it does allow the analytic study of the effects of geometry, magnetic field, and, of more importance, ionic composition on the wake. As discussed in Gurevich et al. [1970, 1973] and Samir et al. [1980], variations in ion composition play a critical role in the details of the expansion of the ion population into the rarefied wake region behind the satellite. Although these results are useful, in most practical situations a finite Debye length is a necessary assumption. This greatly complicates any theoretical computation and requires the advanced probe theory of Section 7.4.4.

An application of analytic probe theory based on local current balance is in the so-called circuit models. The single probe theory introduced so far does not explicitly consider the problem that satellites consist of a variety of surfaces, including dielectrics, and that each surface can charge to a different potential if isolated from the others. In order to explicitly model this differential charging effect, the coupling currents between surfaces must be included in Equation (7.9). Circuit models [Robinson and Holman, 1977; Inouye, 1976; Massaro et al., 1977], as this class of models is termed, consist of many “probes,” each representing a particular point or surface on the satellite (a dielectric surface, for example, would be approximated by one or more individual points). Besides the ambient, secondary, back-scattered, and photoelectron currents considered in the single probe model, the coupling currents to each point, J_{RLC} , are included in J to estimate the currents between surfaces. Time variations are explicitly handled by including inductive and capacitive elements which have finite charging times (local current balance with space is assumed at each instant in time) making these models applicable to a wider range of problems than the single probe models. Inouye [1976] and Massaro et al. [1977] have utilized such models to assess the effects of geomagnetic storm variation, varying solar angle, isotropic fluxes, etc., on individual satellite surfaces as a function of time. Their results, although subject to the difficulties associated with simple probe analysis, indicate

that dielectric surfaces can charge in tens of minutes but may take hours to discharge. Further, charge up can be a long term (days) process and be dependent on the time history.

7.4.4 General Probe Theory

Whereas analytic probe theory is applicable to a number of practical problems, it does not allow for the complex geometric and space charge effects of the satellite sheath on particle trajectories. As a consequence, it is severely limited in its quantitative accuracy (the parametrization method of Cauffman [1973]; Cauffman and Maynard [1974], is one qualitative means of studying these effects using analytic probe theory). In order to include the effects of the sheath on particle trajectories, it is necessary to seek simultaneous, self-consistent solutions of Equations (7.10) and (7.11). Typically, this is not analytically possible and an iterative procedure must be employed. First, $V(\mathbf{r})$ is assumed so that $f_i(\mathbf{r}, \mathbf{v})$ can be computed subject to Equation (7.10). The number densities, n_i , are then found from

$$n_i(\mathbf{r}) = \iiint f_i(\mathbf{r}, \mathbf{v}) d^3V. \quad (7.26)$$

Given the $n_i(\mathbf{r})$, $V(\mathbf{r})$ is computed according to Equation (7.10). The process is iterated until a consistent set of value of $n_i(\mathbf{r})$, $V(\mathbf{r})$, and $f_i(\mathbf{r}, \mathbf{v})$ at grid points surrounding the surface are found. Then the J_i 's at the surface r_s are found from the generalized form of Equation (7.4)

$$J_i(\mathbf{r}_s) = q_i \iiint \mathbf{v} \cdot \mathbf{n} f_i(\mathbf{r}_s, \mathbf{v}) d^3V. \quad (7.27)$$

The theories to be discussed assume the time-independent form of the Vlasov equation. Equation (7.10) is then just a restatement of Liouville's theorem, namely, that $f_i(\mathbf{r}, \mathbf{v})$ is constant along a particle trajectory in a potential $V(r)$. To determine $f_i(\mathbf{r}_p, \mathbf{v})$ at a point \mathbf{r}_p for a particle of a given energy, all that is required is to find the intersection of that particle's trajectory with a surface where f_i is known. The trajectory may either be traced from the point backwards to the surface (the inside-out procedure) or from a surface to the point (outside-in procedure). According to Parker [1976a], the inside-out trajectory tracing method is preferable in that the points at which the density is calculated can be picked at random and is suitable for both electrons and ions. It has the disadvantage that the trajectory information computed for a given point is lost in moving to the next, increasing the computer time. The outside-in method can be readily adapted to time-dependent simulations but introduces difficulties in choosing trajectories so that the density at an arbitrary point can be determined. As a result

many time-consuming trajectory calculations are required. The computation can be greatly reduced, however, by using the "flux tube" method. As Parker [1976a] notes, this adaptation of the outside-in method, in which all the particle trajectories between two reference trajectories are assumed to be similar, ignores the possibility of orbit crossings or reversals and is only suitable for axisymmetric bodies and cold ion beams [Davis and Harris, 1961]. Unless otherwise stated Parker's inside-out method is assumed in the following. The integration of Equation (7.26) then reduces to determining the limits on the trajectories that intersect r_p as these will be the limits on the integral.

The precise method of determining the trajectories that intersect r_p differentiates the various probe calculations [Parker, 1978b, 1980]. Common to all, however, is the so-called orbit classification scheme. Consider the following arguments from classical mechanics (see for example, Goldstein [1965], Bernstein and Rabinowitz [1959], Whipple [1976a], Parker [1977, 1980]). The equation for energy conservation in a spherically symmetric potential $V(r)$ is

$$E = \left[q_i V(r) + \frac{L^2}{2mr^2} \right] + \frac{1}{2} m v_r^2 \quad (7.28)$$

where E is total energy, L is $m v_{ar} =$ angular momentum, v_a is total tangential velocity, and v_r is radial velocity.

The two terms in brackets are called the "equivalent (or effective) potential" $U(r,L)$ [Goldstein, 1965]. For illustration assume the potential $V(r)$ is attractive and of the form

r^{-1} . For various values of L we find that U has the shapes plotted in Figure 7-20a. Looking at the contour L_p , four types of orbits can be defined relative to point $r = r_s$. Adopting the terminology of Parker [1973, 1980], they are (Figure 7-20b) as follows:

Type 1: The particle has sufficient kinetic energy and small enough angular momentum to reach r_s from infinity or to reach infinity from point r_s . These orbits would contribute only once to a density integral at r_s .

Type 2: The particle starts at infinity but never reaches r_s , being repelled at some minimum distance. If the minimum distance is inside the region being integrated over, it contributes twice as it goes both in and out [Parker, 1980] and zero if it is outside the region of interest.

Type 3: The particle starts at r_s , but is reflected at some distance back to r_s . These particles contribute twice to the integral if r_s lies outside the turning point.

Type 4: Type 4 orbits are trapped orbits that circulate around the satellite. These are normally ignored as the orbits can only be populated by collisions that are assumed zero in most satellite studies. As Parker [1980] notes, this assumption has never been justified rigorously.

As a specific example of these calculations, we will review the spherically symmetric models of Parker [1973, 1975, 1976b, 1980]. These models have been successfully compared to the "Equivalent Potential Formulation" [Parker, 1975] and the particle-pushing code of Rothwell et al. [1976] (Figure 7-23a). The typical procedure follows. Assuming spherical symmetry, Equations (7.26) and (7.27) can be reduced to two-dimensional integrals. It is also more

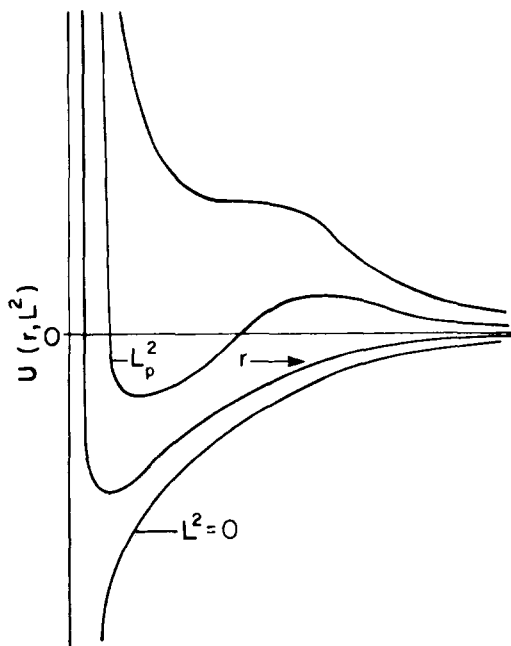


Figure 7-20a. The "equivalent potential" $U(r,L)$ as a function of r for various values of L .

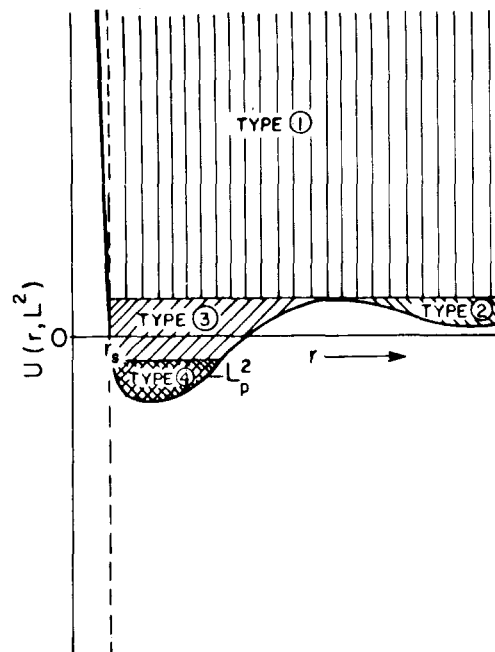


Figure 7-20b. Same as a, only for the L_p contour illustrating the four classes of orbits.

CHAPTER 7

convenient to work in terms of E and L^2 so that the equations become

$$n_i(r) = \frac{\pi}{m^2 r^2} \iint \frac{f_i(E, L^2) dE dL^2}{(2m [E - q V(r)] - L^2/r^2)^{1/2}} \quad (7.29a)$$

$$J_i(r) = \frac{q \pi}{m^3 r^2} \iint f_i(E, L^2) dE dL^2. \quad (7.29b)$$

The integrations are now over the allowable ranges of E and L^2 .

There are two common ways of defining the allowable range of integration in the (E, L^2) space. The first scheme makes use of the fact that the energy E must be greater than $U(r)$ if the trajectories are to exist:

$$E > \left[q_i V(r) + \frac{L^2}{2mr^2} \right] = U(r). \quad (7.30)$$

The maxima are found in $U(r)$. This is the "Effective Potential Formulation" [Parker, 1980] and has been utilized by Bernstein and Rabinowitz [1959], Laframboise [1966], and Chang and Bienkowski [1970].

The other approach is to define a function:

$$g \equiv r^2 [E - q_i V(r)] > \frac{L^2}{2m} \quad (7.31)$$

where g is called the turning point function [Parker, 1980]. To classify the orbits, the minima in g are found. This technique is termed the "Turning-Point Formulation" and has been utilized by Bohm et al. [1949], Allen et al. [1957], Medicus [1961], and Parker [1973, 1975, 1976b]. Although the two methods are equivalent, Parker [1975] indicates that the Turning-Point Formulation is simpler and more efficient.

After obtaining equations of the form of Equations (7.29a) and (7.29b), solutions are found at a given point in space assuming $V(r)$ is known. That is, Equations (7.29a) and (7.29b) are broken up into integrals corresponding to the different orbit types (note that type 4 orbits are normally ignored). $f_i(E, L^2)$ is assumed known at the probe surface (0 for no emission or the appropriate values for secondary or photoelectron emission) and, typically, assumed to be a Maxwellian in the ambient medium.

The next step is to determine the integral bounds on E and L^2 . A typical example in terms of the Turning-Point Formulation is presented in Figure 7-21 [Parker, 1980] and should be compared with Figure 7-20. For a given value of r and E the limits on L^2 are determined. Once the integral ranges of E and L^2 are known for r , $n_i(r)$ and $J_i(r)$ are

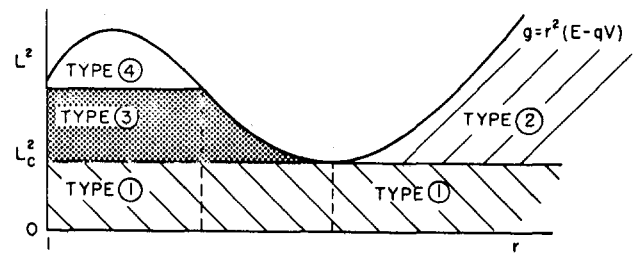


Figure 7-21. Turning-point formulation of Parker [1980]. Example illustrating domains of four types of orbits in (R, LK^2) space. Four in this plot is in units of r_s .

computed. $V(r)$ is found by numerical integration from Poisson's equation given the $n_i(r)$ at grid points around the surface. The process is then iterated until a consistent solution is found. Recently, Parker (1979, 1980) employed the spherically symmetric model to calculate the sheath of a body of radius 100 Debye lengths and for a voltage of 400 000 kT/q, the most extreme combination of size and voltage solved rigorously to date.

More general geometric situations require actual numerical trajectory tracing and are discussed in Parker [1973; 1977; 1978a, b; 1979], Parker and Whipple [1967, 1970], Whipple [1977], and Whipple and Parker [1969a, b]. While the above procedure for spherical symmetry is qualitatively representative of the calculations represented by these papers, numerical particle tracing is required if more realistic geometries such as for the truncated cylinder or "pillbox" illustrated in Figure 7-22 are to be studied. The final potential contours, in this case for a directed plasma flow showing the effects of a wake [Parker, 1978a], arrived at by the iteration process are plotted in Figure 7-22.

The preceding theoretical studies of Parker, Whipple, and others have been particularly useful in studying the effects of differential charging and space-charge potential minima. Differential charging, as distinct from space-charge potential minima, has been demonstrated by these and similar efforts to result from wake effects [Parker, 1967a, 1978a, b], from asymmetric photoelectron emission (see, for example, Grard et al. [1973]; Fahleson [1973]; Whipple [1976b]; Prokopenko and Laframboise [1977b, 1980]; Besse and Rubin, [1980]), and from exposed potentials (Reiff et al. [1980]; Stevens [1980]). The effects of the space-charge potential minimum produced by emitted-electron space charge has been investigated by Soop [1972, 1973], Schroder [1973], Parker [1976b], Whipple [1976a], and Rothwell et al. [1977] [see also Guernsey and Fu, 1970; Grard and Tunaley, 1971; and Grard et al., 1973]. Whipple [1976b] and Parker [1976a] found that such barriers, which are typically a few volts, are inadequate to account for the ATS 6 observations of trapped photoelectrons and secondaries, and that a differential charging barrier must be invoked. Such charging barriers can significantly affect observations and their existence must be considered in designing satellite instrumentation.

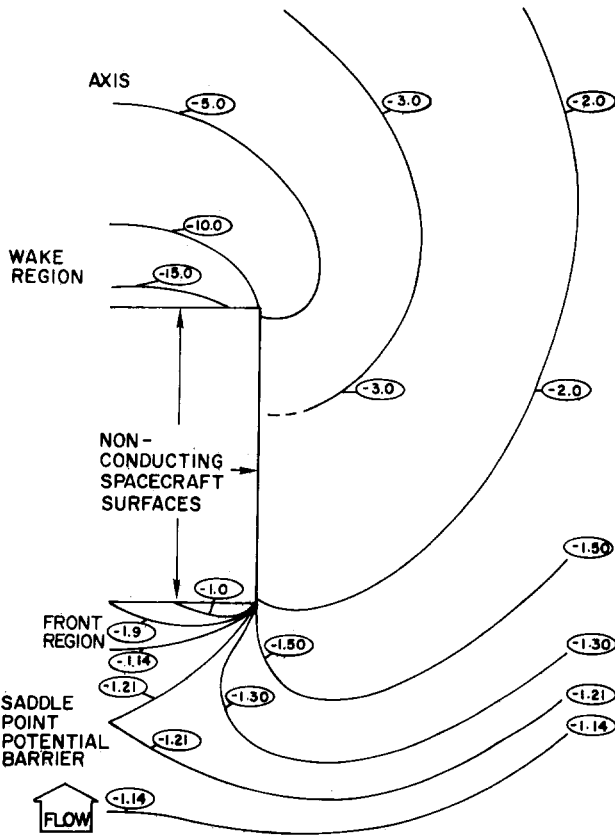


Figure 7-22. Differential charging of nonconducting spacecraft by directed plasma flow (equipotential contours are in units of kT/q) [Parker, 1978a].

7.4.5 Numerical Simulation Techniques

Although general probe theory can be applied to a number of interesting and important cases, it has not been extended much beyond spherical or cylindrical geometries nor does it take into consideration time variations in the sheath. Numerical techniques have been developed that, though retaining many of the basic concepts of probe theory, allow explicit inclusion of time dependency or geometry. These models are capable of handling time variations on the order of the plasma frequency or complex shapes such as the shuttle or the P78-2 SCATHA satellite.

The most straightforward numerical techniques conceptually, though perhaps the most demanding computationally, are the so-called "particle pushing" codes. As originally presented by Albers [1973] and Rothwell et al. [1976, 1977] for a spherical geometry and by Soop [1972, 1973] and Mazzella et al. [1979] for cylindrical geometry, many individual or groups of similar particles are followed simultaneously by computer as they move through the satellite sheath. At each time step the potential on a given particle or set of particles due to all the other particles is computed by a fast Poisson equation solver. The particle group is

incremented in time using this net potential. The next group is then moved based on the other particles. The process is iterated in time with the computer keeping track of surface interactions (backscattered and secondary electrons, photoelectrons, and the outer boundary) and interactions between the satellite fields and the particles. Although plasma simulation codes of this type have been extensively employed in plasma physics, they are just beginning to be used for the plasma probe problem.

Although still limited by computer capacity to relatively simple spherical and cylindrical geometries, these models have been invaluable in studying the detailed effects of space charge and the time-history of the plasma sheath. Results for a spherical model of this type from Rothwell et al. [1976, 1977] are presented in Figures 7-23a and b. Of considerable interest are comparisons in Figure 7-23a between the code and a steady state solution for the case of strong electron emission [the "PARKSSG" code of Parker, 1976b]. The probe in this case was biased at +2 V and the electrons emitted at an energy of 1eV, the other parameters are as indicated (secondary emission has been ignored). The results are meant to resemble isotropic photoemission and show very good agreement between the two very different types of codes. Figure 7-23b illustrates the important ability that such codes have in simulating the time-dependent behavior of satellite charging following the turn-on of photoemission as a function of different ambient conditions. The rapid (2–10 μ s) rise time of the probe in response to

STRONG EMISSION COMPARISON OF STEADY STATE (PARKSSG) WITH TIME SIMULATION (AFGL - SHEATH)

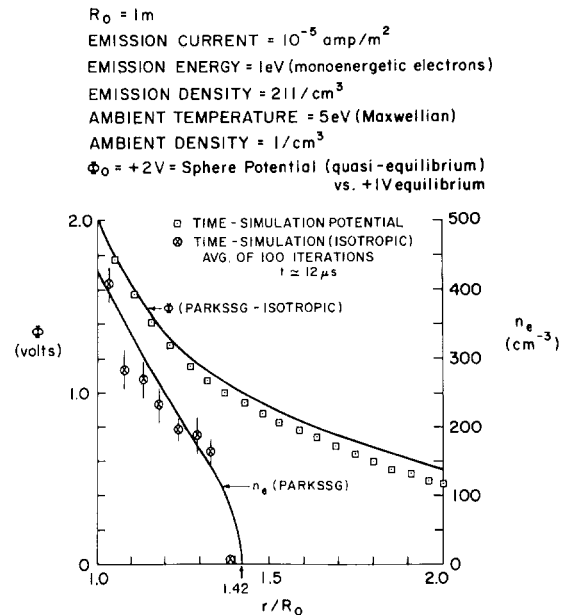


Figure 7-23a. Comparison of steady state sheath potential and density for 2 models: the steady state PARKSSG code and the AFGL-SHEATH code [Rothwell et al., 1977].

SATELLITE POTENTIAL FOR A STRONG PHOTOEMISSION AND VARIOUS AMBIENT PLASMA DENSITIES

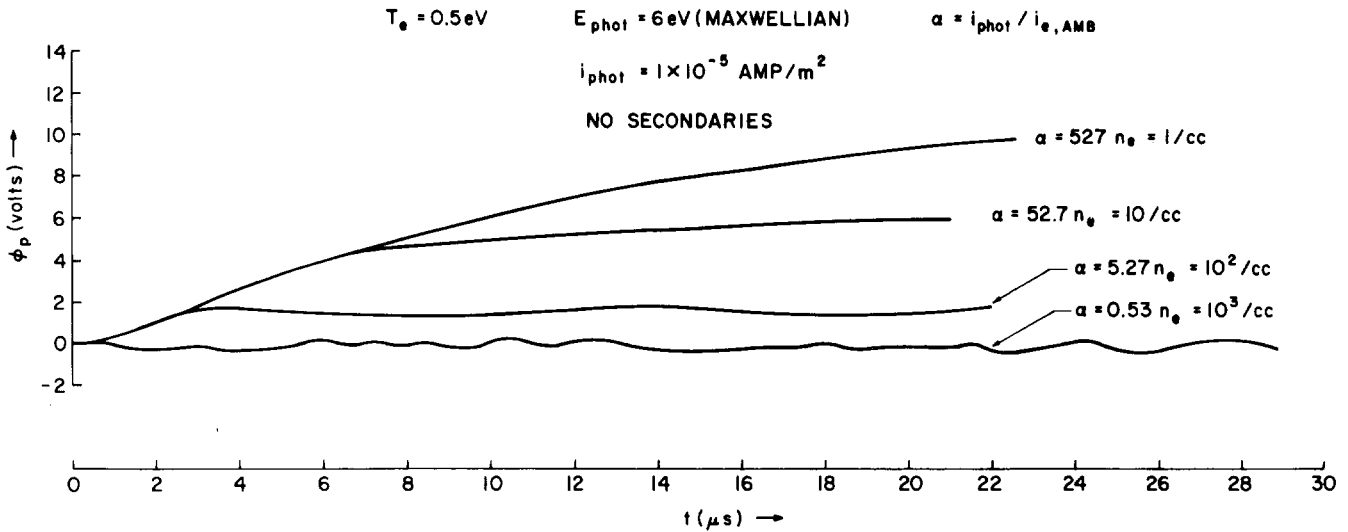


Figure 7-23b. Spacecraft voltage transients following the “turn-on” of the plasma at $t = 0$. The results are for a sphere (no secondary emission). α is the ratio of photoelectron to ambient electron temperature, and E_{phot} is the mean energy of the photoelectrons assumed to be Maxwellian [Rothwell et al., 1977].

the turn-on of photoemission could be significant in causing satellite transients as only $\sim 2 \text{ V}$ are necessary to trigger many circuits.

The cylindrical, particle pushing code AFSIM (*Air Force Satellite Interactions Model*) [Mazzella et al., 1979] has been employed to follow the effects of an electron beam emitted by a satellite. A 300 eV beam at 200 μA was emitted into a vacuum from a satellite initially at 0 potential. The computations showed that the satellite potential rose to +300 V at 36 μs , at which point a portion of the beam was trapped in the sheath and began to orbit the satellite. A space-charge potential formed four spacecraft radii away with most of the beam being reflected back to the satellite. Figure 7-24 shows the configuration 65 μs after turn on. The circle represents the satellite and the beam is visible as a collimated source while the comet-like structure to the right is the cloud of previously trapped beam electrons orbiting the satellite.

7.4.6 NASCAP

Particle pushing codes are very useful in studying the detailed behavior of particles in time and in the sheaths surrounding a probe. They are still, however, limited to relatively simple geometries because of computer limitations and are subject to numerical instabilities. Recently an alternative model has become available that explicitly treats the effects of geometry. This is the NASCAP (*NASA Charging Analyzer Program*) computer code [Katz et al., 1977,

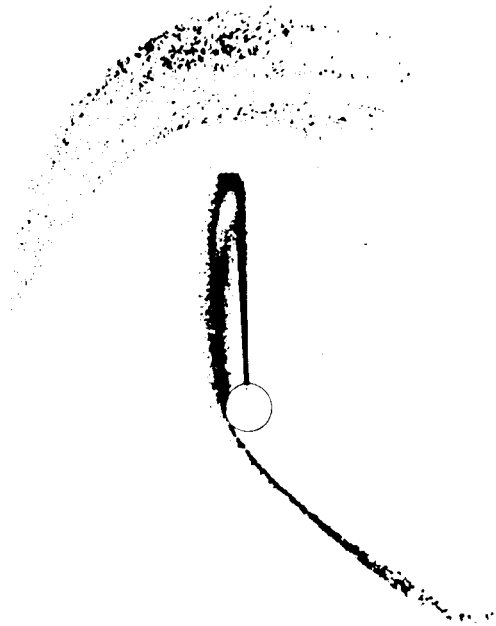


Figure 7-24. Sheath simulation using the AFSIM code [Mazzella et al., 1970] at 65 μs after turn-on of a 30 eV, 200 μA electron beam.

CHARGING OF SPACECRAFT SURFACES

1979; Schnuelle et al., 1979; Roche and Purvis, 1979; Rubin et al., 1980] for the thick sheath limit (the model is currently being extended to thin sheaths). This code combines a solution of the Poisson equation and a probe charging model along with a complex graphics package to compute the detailed time behavior of charge deposition on spacecraft surfaces. An approximate circuit model of the satellite is used to estimate voltage changes during time steps for an implicit potential solver. The propagation of particle beams through the satellite sheath is computed by orbit tracing in the sheath field. The code has several options available ranging from a less-detailed code capable of calculating the differential potential on a simple laboratory material sample to a detailed code capable of modeling individual booms and sensor surfaces on a complex satellite such as the P78-2 SCATHA satellite [Rubin et al., 1980]. The primary intent of the model is to compute the effects of satellite geometry on the satellite photosheath, sheath field, and surface material potentials.

The first step in the NASCAP model is to insert the satellite geometry and material content. Using simple 3-dimensional building blocks, the code has provisions for modeling surfaces ranging from cubes and planes to complete satellites with their booms and solar panels (Figure 7-25a). In the second stage the currents to the satellite surfaces are computed by treating each surface element as a current-collecting probe. The inside-out technique may then be used to model the charge distribution in the photosheath. The program is stepped forward in time, local current balance being assumed at each time step. Time-dependency and variations in differential potential can thus be modeled as demonstrated in Figure 7-25b. The analysis is carried out on successively larger, coarser nested grids [Katz et al., 1977], allowing the trajectories of particles emitted from the satellite to be traced in the space surrounding the satellite (Figure 7-25c).

The NASCAP program combines the best elements of

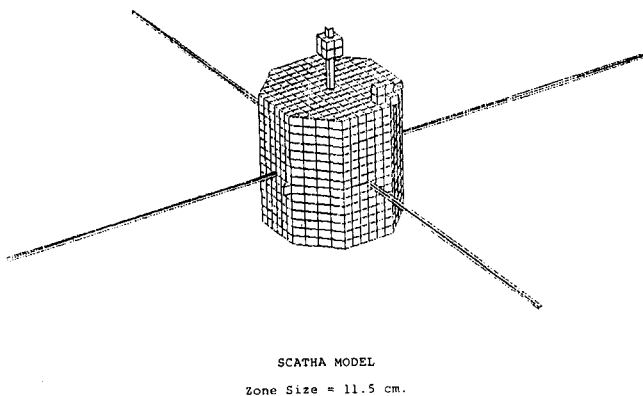


Figure 7-25a. NASCAP computer simulation of the P78-2 SCATHA satellite [Schnuelle et al., 1979]. Compare with Figure 7-6.

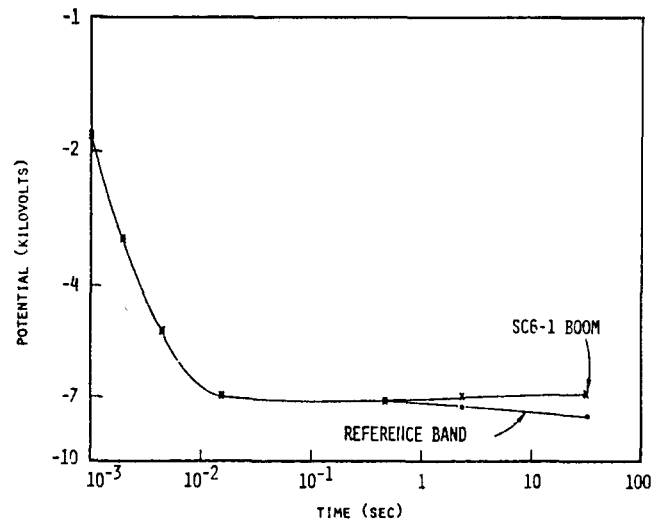


Figure 7-25b. NASCAP computer simulation time-dependence of potential for two surfaces on the P78-2 SCATHA satellite [Schnuelle et al., 1979].

the circuit element model, the inside-out technique, and Langmuir probe theory in one model along with the added advantage of detailed graphical results. Unfortunately, with this gain in capability, the code has become large and requires hours of computing time for the more detailed models. Two steps have been taken to alleviate these problems. First, efficient versions have been developed for specific com-

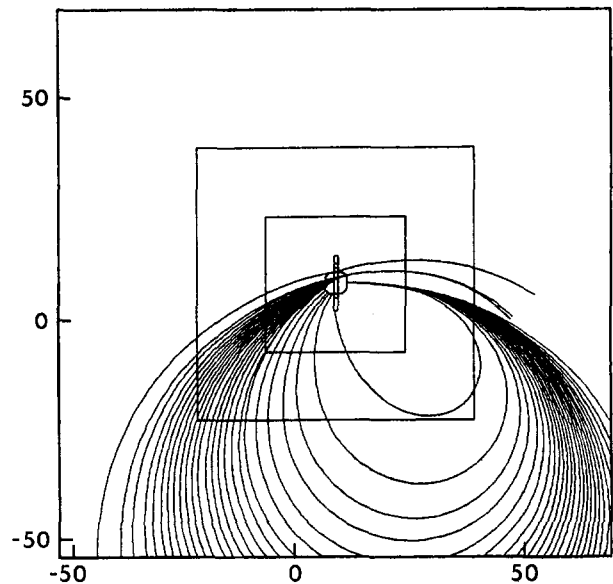


Figure 7-25c. Particle trajectories from an electron emitter as computed by the NASCAP code in the presence of a magnetic field [Rubin et al., 1980]

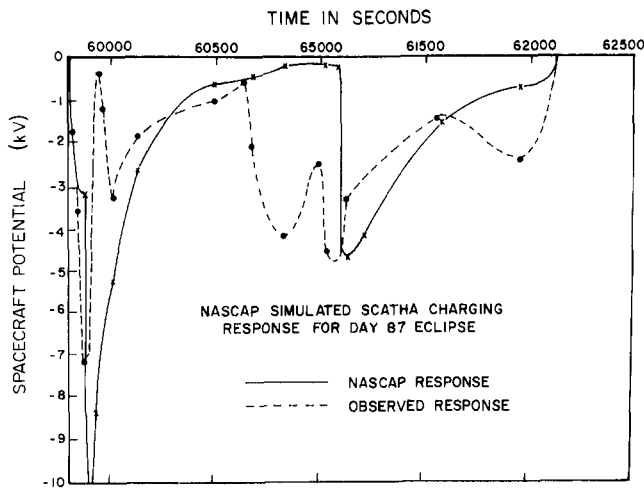


Figure 7-26a. Observed satellite to space potential (P78-2 SCATHA) between 1630 and 1730 UT on day 87, 1979. Also shown are NASCAP predictions for the same period [Schnuelle et al., 1981].

putational tasks such as the SCATHA version discussed in Rubin et al. [1980]. Secondly, in conjunction with a number of laboratory and *in situ* satellite experiments, an attempt is being made to verify all aspects of the code and determine what are the critical input parameters [Purvis et al., 1977; Roche and Purvis, 1979; Stevens et al., 1980a]. The model has been applied to many satellite charging problems such as large cavities, exposed potentials, and arbitrary geometries not considered previously [Purvis, 1980; Stevens, 1980; Stevens and Purvis, 1980].

Preliminary results of comparisons between the P78-2 SCATHA measurements and NASCAP have recently become available. Some of these results are plotted in Figures 7-26a and 7-26b. In Figure 7-26a [Schnuelle et al., 1981], the observed satellite to space potential between 1630 and 1730 UT on day 87, 1979 is plotted. The data, consisting of potential and plasma measurements during an eclipse, were input into the NASCAP “one-grid” model (as the name implies, this computation makes use of only the inner most NASCAP computational grid—Figure 7-25c) at ~1 minute (1 spin period) intervals. Although the NASCAP simulation misses the two minor jumps in potential, it reproduces the two major ones and is in excellent quantitative agreement with the data considering the uncertainties in material properties. NASCAP also responds more slowly to environmental changes than the actual data. As Schnuelle et al. [1981] note, this is due to the 1 minute time steps imposed on NASCAP by the data whereas the real environment is changing continuously.

Figure 7-26b [Stevens et al., 1980c], comparing the NASCAP predictions with the surface potential of a Kapton sample (SC1-2—see Table 7-1) on P78-2-SCATHA, is interesting for two reasons. First, it illustrates kV changes in

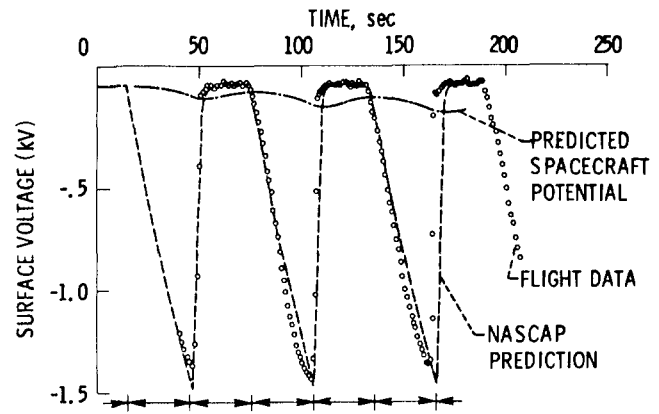


Figure 7-26b. Observed potential difference measured by the P78-2 SCATHA satellite surface potential monitor experiment between a Kapton sample and the satellite ground. Also shown are NASCAP predictions from same period [Stevens et al., 1980a].

the potential between the Kapton and the satellite ground at the spin frequency of the satellite. Second, it illustrates the power of NASCAP in predicting such rapid variations (the slight time-lag between the data and theory is due to the actual satellite spin period being slightly faster than the assumed 1 rpm). This agreement is, in part, much better than the prediction of the satellite to space potential as the Kapton sample properties were obtained prior to flight in ground test simulations—an important consideration in future studies.

7.5 PREVENTION OF SPACECRAFT CHARGING

Although varying the satellite to space potential allows the measurement of very low energy plasma, charge buildup on satellite surfaces is not in general a desired phenomenon. In order to eliminate or at least limit the worst effects of spacecraft charging, several techniques have been developed. Although the obvious solution is to develop systems that can withstand the worst effects, this is not always a feasible or desirable method. Alternatives to this “brute force” method will be described in this section.

The simplest method for preventing spacecraft charging effects is to employ sound design techniques—use conducting materials where possible and proper grounding techniques. These techniques are detailed in a design guideline handbook recently completed at NASA Lewis [Purvis et al., 1984]. Although a large satellite to space potential can occur, differential charging, the major spacecraft charging problem, is significantly reduced by these procedures. Several different methods have been developed to assure an adequately conducting surface. As an example, non-conducting surfaces on the GEOS series of geosynchronous

CHARGING OF SPACECRAFT SURFACES

satellites were coated with indium oxide. As solar cells are the primary non-conducting surfaces on GEOS and as indium oxide is sufficiently transparent to sunlight so that it does not degrade their operation, this technique has been quite successful [G.L. Wrenn, private communication, 1980] at keeping satellite differential potentials near zero and, because of the secondary emission properties of indium oxide, the satellite to space potential between zero and -1000 V even in eclipse. Such coating techniques, however, can be expensive and difficult if large surfaces are involved. Furthermore, they do not reduce the hazards associated with charge deposition in dielectrics and, in the case of "pinholes" (Section 7.3.8), may be ineffective.

Another technique that may be applicable to large surfaces involves the use of electron and ion emitters. Grard [1977] and Gonfalone et al. [1979] discussed the application of such systems to actual satellite systems. The latter paper described the successful application of a low current (mA) electron emitter on the ISEE-1 satellite. The ISEE-1 is in a highly elliptical (300 km to $23 R_E$) orbit so that it spends a long time in the solar wind. The ISEE-1 results indicated that the electron cloud emitted by the satellite gun successfully clamped the potential of the satellite at a few volts positive to the ambient solar wind plasma. Purvis and Bartlett [1980] reported results from ion and electron emitters on the geosynchronous ATS 5 and ATS 6 satellites. These results indicated that whereas electron emission alone reduced the satellite to space potential to ~ 0 , it did not significantly reduce the charge on dielectrics. Use of an ion emitter and neutralizer together not only clamped the satellite to space potential at 0, but also, through the cloud of ions, neutralized the negative charge on the dielectrics. Similar success was demonstrated by the beam experiments on the P78-2 SCATHA satellite [H.A. Cohen, private communication, 1980]. There may be some difficulties, however, with these techniques as reducing the surface charge may enhance dielectric breakdown [A.R. Frederickson, private communication, 1980] between the deposited charge and the surface. Also there is the possibility of contamination of the satellite environment by the beam ions.

Careful selection of satellite materials can reduce spacecraft charging. Although thermal control surfaces which are necessary on many satellites generally consist of dielectric materials, careful selection of the materials according to their secondary emission properties and bulk conductivity can reduce charge buildup. Rubin et al. [1978] have demonstrated that for materials with a secondary emission greater than 1, the plasma temperature must be several times the energy at which this occurs if a satellite is to charge up. Again, however, the increased secondary electron population could contaminate low energy ($E \lesssim 10$ eV) plasma observation.

Several other techniques have been proposed (for example, see Beattie and Goldstein [1977] for methods of protecting the Jupiter probe) and recent results indicate that

dielectric materials may be altered by the arcing process in a manner which greatly reduces future arcing [A.R. Frederickson, private communication, 1980]. It is currently thought, however, that the techniques described above are adequate in reducing charging. Basically, spacecraft charge prevention is a matter of good design technique—ground well, avoid cavities in which charge can be deposited, and avoid exposed potentials.

7.6 CONCLUSIONS

Before concluding this chapter, a brief summary of the major accomplishments of this fourth period of charging analysis is in order. Probably the major step forward has been the growing realization by the space physics community of the role of spacecraft charging. Before the geosynchronous observations of 10(kV) and higher potentials, spacecraft charging was considered to be a nuisance. Since that time, however, spacecraft charging analysis has become an important adjunct to plasma experiments and to satellite design. On the negative side, however, there is still apparent confusion on the part of some experimentalists as to how to correct low energy measurements and an unwillingness on the part of satellite designers to spend the necessary time in properly designing their satellites. Both of these problems have proven hard to solve.

In the area of plasma measurements, the spacecraft charging theory necessary for their interpretation can be said on the basis of this review to be quite sophisticated. The simple probe theory of Langmuir and his successors has been shown to give adequate order of magnitude estimates of the gross effects of spacecraft charging. The introduction of various sophistications such as the satellite velocity or the satellite sheath [Cauffman and Maynard, 1974, for example] have made this theory applicable to many practical cases. The development of finite element models has allowed fairly sophisticated engineering studies. The original methods of Bernstein and Rabinowitz have grown into the intricate, advanced trajectory codes of Parker, Whipple, and others. In combination with various simplifications these techniques have yielded straightforward methods of correcting Langmuir probe data. Even secondary emission, photoelectron emission, and velocity effects can be modeled.

With the advent of electrostatic analyzers and their ability to provide both detailed spectral information and mass discrimination, experimental information on charging effects has increased enormously. As a result, active studies of the sheath population and fields in the vicinity of a spacecraft under a variety of ambient conditions have become feasible. These have been carried out in detail on the GEOS and P78-2 SCATHA satellites for the geosynchronous orbit. Similar experiments are planned for the early shuttle payloads. Theoretical models of the sheaths and fields around

CHAPTER 7

typical geosynchronous satellites are available, ranging from the simple thick sheath probe models to the NASCAP code which is capable of handling complex geometries. Advanced wake and sheath models are also available for shuttle studies. Rapid time variations on the order of the plasma frequency have even been modeled.

In the area of engineering design, finite element models have been applied in the design of a number of geosynchronous and interplanetary missions. NASCAP has been applied to several systems and proven useful in designing vehicles so as to avoid the worst effects of charging. On the practical side, effort is beginning to be expended in developing charge-reducing materials and techniques. More importantly, the techniques learned on small spacecraft are beginning to be applied in the design of the next generation of large, high voltage vehicles.

Despite this impressive growth of spacecraft charging technology since 1965, there are still a number of areas in need of study. These can be grouped under the headings of material properties, geometry, magnetic fields, wakes, arcs, large size/high potential, and charge deposition in dielectrics. Although work is under way in each of these areas, much still remains to be accomplished. Even so, more than enough has been accomplished in this fourth stage of spacecraft charging analysis so that, as a scientific discipline, spacecraft charging can be said to have come of age.

APPENDIX—Table 7-3 Explanation

The simple probe models of Section 7.4.1. can give first order estimates of the satellite to space potential under a variety of conditions. Given the plasma parameters listed in Table 7-3, this potential has been estimated using approximations to Equations (7.22) and (7.24). As only a first order estimate is desired, a conducting spherical satellite (~ 1 m in diameter) has been assumed. Secondary and backscatter terms are ignored (these would tend to make the potential more positive). For the planar, thin sheath assumption (1-D in Table 7-3): [T is in eV.]

$$V = \frac{-T_E}{q} \text{Ln} \left(\frac{I_{EO}}{I_{IO} + I_{PH}} \right) \quad V < 0$$

$$V = \frac{-T_I}{q} \text{Ln} \left(\frac{I_{EO} - I_{PH}}{I_{IO}} \right) \quad V > 0$$

For the spherical, thick sheath assumption (3-D in Table 7-3):

$$V = \frac{-T_E}{q} \text{Ln} \left[\frac{I_{EO}}{I_{IO} \left(1 - q \frac{V}{T_I} \right) + I_{PH}} \right] \quad V < 0$$

$$V = \frac{-T_I}{q} \text{Ln} \left[\frac{I_{EO} \left(1 + q \frac{V}{T_E} \right) - I_{PH}}{I_{IO}} \right] \quad V > 0$$

where:

$$I_{EO} = 4\pi r_s^2 \cdot \frac{qn_{EO}}{2} \left(\frac{2T_I}{\pi m_E} \right)^{1/2}$$

$$I_{IO} = 4\pi r_s^2 \cdot \frac{qn_{IO}}{2} \left(\frac{2T_I}{\pi m_I} \right)^{1/2}$$

$$I_{PH} \approx \pi r_s^2 \cdot J_{PHO} / (1 + V/0.7)^2 \quad V > 0$$

$$\approx \pi r_s^2 \cdot J_{PHO} \quad V < 0$$

r_s = satellite radius

For the "RAM" case and assuming a thin sheath for the electrons:

$$V = \frac{-T_E}{q} \text{Ln} \left(\frac{I_{EO}}{I'_{IO} + I_{PH}} \right) \quad V < 0$$

$$V = \left[1 - \left(\frac{I_{EO} - I_{PH}}{I'_{IO}} \right) \right]^{1/2} m_I v_s^2 q^{-1} \quad V > 0$$

Where: $I_{IO} = \pi r_s^2 \cdot qn_{IO}v_s$

v_s = satellite velocity

This assumes, for ion repulsion, that the ion ram current, I_{IO} , is reduced by a factor $(1 - qV^{1/2}/m_I v_s^2)$ and that the ions have ~ 0 thermal velocity (see Whipple [1965], p. 28).

The assumed environmental parameters have been adopted from many sources. They should be treated at best as rough approximations as the actual environments can vary by factors of $\times 10$ to $\times 100$. The Jupiter data are from Scudder et al. [1981] and J. Sullivan [private communication]. The solar wind data for less than 1 AU are from Schwenn et al. [1977]. Values greater than 1 AU are estimated.

ACKNOWLEDGMENTS

This work represents the conclusion of 5 years of work at the Air Force Geophysics Laboratory. During that time, my main source of advice and direction was C.P. Pike. Grateful appreciation is also extended to A. Rubin, P. Rothwell, L.W. Parker, and N. Saffekos, who helped me learn the intricacies of spacecraft charging. N.J. Stevens and C. Purvis have provided much practical assistance and advice. T. Gindorf, P. Robinson, E.C. Whipple, Jr., and P. Leung helped in the final revision. M. Spanos and B. Short prepared the transcript. Finally, K. Garrett provided much needed physical support through the long hours expended in producing the manuscript. The work described in this chapter was carried out in part at the Jet Propulsion Laboratory, California Institute of Technology, under NASA contract NAS7-100.

REFERENCES

- Ahmed, M. and R.C. Sagalyn, "Thermal Positive Ions in the Outer Ionosphere and Magnetosphere from OGO 1," *J. Geophys. Res.*, **77**: 1205-1220, 1972.
- Albers, N., "Computer Simulation of a Spherical Langmuir Probe," *SU-IPR Report 449*, Stanford University, Calif., 1973.
- Allen, J.E., R.L.F. Boyd, and P. Reynolds, "The Collection of Positive Ions by a Probe Immersed in a Plasma," *Proc. Phys. Soc. London*, **70**: 297-304, 1957.
- Al'pert, J.L., Wave-Like Phenomena in the Near-Earth Plasma and Interactions with Man-Made Bodies," in *Handbuch Der Physik*, edited by S. Flugge, *Geophysics III, Part V*, 217-350, Springer-Verlag, Berlin 1976.
- Al'pert, J.L., A.V. Gurevich, and L.P. Pitaevskii, *Space Physics with Artificial Satellites*, Consultants Bureau, New York, 186-210, 1965.
- Balmain, K.G., "Surface Discharge Effects," in *Space Systems and Their Interactions with the Earth's Space Environment*, (*Prog. Astronaut. Aeronaut.*, **71**) edited by H.B. Garrett and C.P. Pike, 276-298, AIAA Press, New York, 1980.
- Balmain, K.G., M. Cuchanski, and P.C. Kremer, "Surface Micro-Discharges on Spacecraft Dielectrics," in *Proceedings of the Spacecraft Charging Technology Conference*, edited by C.P. Pike and R.R. Lovell, AFGL TR-77-0051/NASA TMX-73537, ADA045459, 519-526, 1977.
- Baragiola, R.A., E.V. Alonso, and A.O. Florio, "Electron Emission from Clean Metal Surfaces Induced by Low-Energy Light Ions," *Phys. Rev. B*, **19**: 121-129, 1979.
- Beard, D.B. and F.S. Johnson, "Charge and Magnetic Field Interaction with Satellites," *J. Geophys. Res.*, **65**: 1-7, 1960.
- Beard, D.B. and F.S. Johnson, "Ionospheric Limitations on Attainable Satellite Potential," *J. Geophys. Res.*, **66**: 4113-4122, 1961.
- Beattie, J.R. and R. Goldstein, "Active Spacecraft Potential Control System for the Jupiter Orbiter with Probe Emission," in *Proceedings of the Spacecraft Charging Technology Conference*, edited by C.P. Pike and R.R. Lovell, AFGL TR-77-0051/NASA TMX-73537, ADA045459, 143-165, 1977.
- Bernstein, I.B. and I.N. Rabinowitz, "Theory of Electrostatic Probes in a Low-Density Plasma," *Phys. Fluids*, **2**: 112, 1959.
- Bernstein, W., et al., "Electron Beam Experiments: The Beam Plasma Discharge at Low Pressures and Magnetic Field Strengths," *Geophys. Res. Lett.*, **5**: 127-130, 1978.
- Bernstein, W., H. Leinbach, P.J. Kellogg, S.J. Monson, and T. Hallinan, "Further Laboratory Measurements of the Beam-Plasma Discharge," *J. Geophys. Res.*, **84**: 7271-7278, 1979.
- Beers, B.L., et al., "First Principles Numerical Model of Avalanche-Induced Arc Discharges in Electron-Irradiated Dielectrics," *NASA-C-168* (Rev. 10-75), 1979.
- Besse, A.L. and A.G. Rubin, "A Simple Analysis of Spacecraft Charging Involving Blocked Photoelectron Currents," *J. Geophys. Res.*, **85**: 2324, 1980.
- Bohm, D., "Minimum Ionic Kinetic Energy for a Stable Sheath," in *The Characteristics of Electrical Discharges in Magnetic Fields*, edited by A. Guthrie and R.K. Wakerling, 77-86, McGraw-Hill, New York, 1949.
- Bohm, D., H.S. Burhop, and H.S.W. Massey, "The Use of Probes for Plasma Exploration in Strong Magnetic Fields," in *Characteristics of Electrical Discharges in Magnetic Fields*, edited by A. Guthrie and R.K. Wakerling, McGraw-Hill, New York, 1949.
- Bourdeau, R.E., "On the Interaction Between a Spacecraft and an Ionized Medium," *Space Sci. Rev.*, **1**: 719-728, 1963.
- Bourdeau, R.E., J. L. Donley, G.P. Serbu, and E.C. Whipple Jr., "Measurement of Sheath Current and Equilibrium Potential on the Explorer VIII Satellite," *J. Astron. Sci.*, **8**: 65-73, 1961.
- Brundin, C.L., "Effects of Charged Particles on the Motion of an Earth Satellite," *AIAA J.*, **1**: 2529-2538, 1963.
- Cambou, F., R.Z. Sagdeev, and I.A. Zhulin, "Reviewing Artificial Radiation and Aurorae Between Kerguelen and Soviet Union," *Space Sci. Instrument.*, **4**: 117-121, 1978.
- Cauuffman, D.P., "Ionization and Attraction of Neutral Molecules to a Charged Spacecraft," SAMS0 TR-73-263, 1973.
- Cauuffman, D.P., "The Effects of Photoelectron Emission on a Multiple-Probe Spacecraft Near the Plasmapause," in *Photon and Particle Interactions with Surfaces in Space*, edited by R.J.L. Gard, 153-162, D. Reidel, Dordrecht, Holland, 1973.
- Cauuffman, D.P. and N.C. Maynard, "A Model of the Effect of the Satellite Photosheath on a Double Floating Probe System," *J. Geophys. Res.*, **79**: 2427-2438, 1974.
- Cernuschi, F., "The Physics of Cosmic Grains," *Astrophys. J.*, **105**: 241-254, 1947.
- Chang, K.W. and G.K. Bienkowski, "Effects of Electron Emission on Electrostatic Probes at Arbitrary Pressures," *Phys. Fluids*, **13**: 902, 1970.
- Chang, H.H.C. and M.C. Smith, "On the Drag of a Spherical Satellite Moving in a Partially Ionized Atmosphere," *J. Brit. Interplanet. Soc.*, **17**: 199-205, 1960.
- Chang, J.S., S.M.L. Prokopenko, R. Godard, and J.G. Laframboise, "Prediction of Ion Drift Effects on Spacecraft Floating Potentials," in *Spacecraft Charging Technology—1978*, edited by R.C. Finke and C.P. Piek, NASA CP-2071/AFGL TR-79-0082, ADA084626, 179-187, 1979.
- Chen, F.F., "Electric Probes," in *Plasma Diagnostic Techniques*, edited by R.H. Huddlestone and S.L. Leonard, 113-200, Academic Press, New York, 1965.
- Chopra, K.P., "Interactions of Rapidly Moving Bodies in Terrestrial Atmosphere," *Rev. Mod. Phys.*, **33**: 153-189, 1961.
- Chung, M.S. and T.E. Everhart, "Simple Calculation of Energy Distribution of Low-Energy Secondary Electrons Emitted from Metals Under Electron Bombardment," *J. Appl. Phys.*, **45**: 707, 1974.
- Cipolla, J.W. and M.B. Silevitch, "Analytical Study of the Time Dependent Spacecraft-Plasma Interaction," in *Spacecraft Charging Technology—1978*, edited by R.C.

CHAPTER 7

- Finke and C.P. Pike, NASA CP-2071/AFGL TR-79-0082, ADA084626, 197–208, 1979.
- Cohen, H.A., et al., "Design, Development, and Flight of a Spacecraft Charging Sounding Rocket Payload," in *Spacecraft Charging Technology—1978*, edited by R.C. Finke and C.P. Pike, NASA CP-2071/AFGL TR-79-0082, ADA084626, 80–90, 1979.
- Davis, A.H. and I. Harris, "Interaction of a Charged Satellite with the Ionosphere," in *Rarefied Gas Dynamics*, edited by L. Talbot, 691–699, Academic Press Inc., New York, 1961.
- DeForest, S.E., "Spacecraft Charging at Synchronous Orbit," *J. Geophys. Res.*, **77**: 651, 1972.
- DeForest, S.E., "Electrostatic Potentials Developed by ATS 5," in *Photon and Particle Interactions with Surfaces in Space*, edited by R.J.L. Grard, 263–276, D. Reidel, Dordrecht, Holland, 1973.
- DeForest, S.E. and C.E. McIlwain, "Plasma Clouds in the Magnetosphere," *J. Geophys. Res.*, **76**: 3587–3611, 1971.
- Dekker, A.J. "Secondary Electron Emission," in his *Solid State Physics*, 418–445, Prentice-Hall, Englewood Cliffs, N.J., 1958.
- deLeeuw, J.H., "A Brief Introduction to Ionospheric Aerodynamics," in *Rarefied Gas Dynamics*, edited by C.L. Brundin, **2**:1561–1587, Academic Press, New York, 1967.
- Deutsch, M.-J.C., "Worst Case Earth Charging Environment," *J. Spacecraft*, **19**: 473–477, 1982.
- Durrett, J.C. and J.R. Stevens, "Description of the Space Test Program P78-2 Spacecraft and Payloads," in *Spacecraft Charging Technology—1978*, edited by R.C. Finke and C.P. Pike, NASA CP-2071/AFGL TR-79-0082, ADA084626, 4-10, 1979.
- Evdokimov, O.B. and N.P. Tubalov, "Stratification of Space Charge in Dielectrics Irradiated with Fast Electrons," *Sov. Phys. Solid State*, Engl. Trans., **15**: 1869–1870, 1974.
- Fahleson, U., "Plasma-Vehicle Interactions in Space -- Some Aspects on Present Knowledge and Future Development," in *Photon and Particle Interactions with Surfaces in Space*, edited by R.J.L. Grard, 563–570, D. Reidel, Dordrecht, Holland, 1973.
- Feuerbacher, B., R.F. Willis, and B. Fitton, "Electrostatic Charging and Formation of Composite Interstellar Grains," in *Photon and Particle Interactions with Surfaces in Space*, edited by R.J.L. Grard, 415–428, D. Reidel, Dordrecht, Holland, 1973.
- Finke, R.C. and C.P. Pike (eds.), *Spacecraft Charging Technology—1978*, NASA CP-2071/AFGL TR-79-0082, ADA084626, 1979.
- Frederickson, A.R., "Electric Fields in Irradiated Dielectrics," in *Spacecraft Charging Technology—1978*, edited by R.C. Finke and C.P. Pike, NASA CP-2071/AFGL TR-79-0082, ADA084626, 554–569, 1979.
- Frederickson, A.R., "Radiation Induced Dielectric Charging," in *Space Systems and Their Interactions with the Earth's Space Environment*, (*Prog. Astronaut. Aeronaut.*, **71**) edited by H.B. Garrett and C.P. Pike, 386–412, AIAA Press, New York, 1980.
- Freeman, J.W. Jr., M.A. Fenner, and H.K. Hills, "The Electric Potential of the Moon in the Solar Wind," in *Photon and Particle Interactions with Surfaces in Space*, edited by R.J.L. Grard, 363–368, D. Reidel, Dordrecht, Holland, 1973.
- Garrett, H.B., "Review of Quantitative Models of the 0 to 100 KeV Near-Earth Plasma," *Rev. Geophys.*, **17**: 397–417, 1979.
- Garrett, H.B., "The Charging of Spacecraft Surfaces," *Rev. Geophys. Space Phys.*, **19**: 577–616, 1981.
- Garrett, H.B. and S.E. DeForest, "Time-Varying Photoelectron Flux Effects on Spacecraft Potential at Geosynchronous Orbit," *J. Geophys. Res.*, **84**: 2083–2088, 1979.
- Garrett, H.B. and J.M. Forbes, "A Model of Solar Flux Attenuation During Eclipse Passage and Its Effects on Photoelectron Emission from Satellite Surfaces," *Planet. Space Sci.*, **29**: 601–607, 1981.
- Garrett, H.B. and A.G. Rubin, "Spacecraft Charging at Geosynchronous Orbit—Generalized Solution for Eclipse Passage," *Geophys. Res. Lett.*, **5**: 865, 1978.
- Garrett, H.B., E.G. Mullen, E. Ziemba, and S.E. DeForest, "Modeling of the Geosynchronous Plasma Environment—Part 2, ATS 5 and ATS 6 Statistical Atlas," AFGL TR-78-0304, ADA067018, 1978.
- Garrett, H.B., A.G. Rubin, and C.P. Pike, "Prediction of Spacecraft Potentials at Geosynchronous Orbit," in *Solar-Terrestrial Prediction Proceedings*, edited by R.F. Donnelly, Vol. II, 104–118, U.S. Government Printing Office, 1979.
- Gibbons, D.S., "Secondary Electron Emission," in *Handbook of Vacuum Physics*, 2, edited by A.H. Beck, 301, Pergamon Press, Oxford, U.K., 1966.
- Goldan, P.D., E.J. Yadlowsky, and E.C. Whipple Jr., "Errors in Ion and Electron Temperature Measurements due to Grid Plane Potential Nonuniformities in Retarding Potential Analyzers," *J. Geophys. Res.*, **78**: 2907–2916, 1973.
- Goldstein, H., *Classical Mechanics*, Addison-Wesley, Reading, Mass, 63–69, 1965.
- Goldstein, R. and S.E. DeForest, "Active Control of Spacecraft Potentials at Geosynchronous Orbit," in *Spacecraft Charging by Magnetospheric Plasmas*, (*Prog. Astronaut. and Aeronaut.*, **47**) edited by A. Rosen, 159–168, MIT Press, Cambridge, Mass., 1976.
- Gonfalone, A., A. Pedersen, U.V. Fahleson, C.G. Fälthammar, F.S. Mozer, and R.B. Tobert, "Spacecraft Potential Control on ISEE-1," in *Spacecraft Charging Technology—1978*, edited by R.C. Finke and C.P. Pike, NASA CP-2071/AFGL TR-79-0082, ADA084626, 256–267, 1979.
- Grard, R.J.L. (ed.), *Photon and Particle Interactions with Surfaces in Space*, D. Reidel, Dordrecht, Holland, 1973.
- Grard, R.J.L., "Properties of the Satellite Photoelectron Sheath Derived from Photoemission Laboratory Measurements," *J. Geophys. Res.*, **78**: 2885–2906, 1973b.
- Grard, R.J.L., "The Multiple Applications of Electron Emitters in Space," in *Proceedings of the Spacecraft Charging Technology Conference*, edited by C.P. Pike and R.R. Lovell, AFGL TR-0051/NASA TMX-73537, ADA045459, 203–221, 1977.
- Grard, R.J.L. and J.K.E. Tunaley, "Photoelectron Sheath Near the Planar Probe in Interplanetary Space," *J. Geophys. Res.*, **76**: 2498–2505, 1971.

CHARGING OF SPACECRAFT SURFACES

- Grard, R.J.L., K. Knott, and A. Pedersen, "The Influence of Photoelectron and Secondary Electron Emission on Electric Field Measurements in the Magnetosphere and Solar Wind," in *Photon and Particle Interactions with Surfaces in Space*, edited by R.J.L. Grard, D. Reidel, Dordrecht, Holland, 163–192, 1973.
- Grard, R.J.L., S.E. DeForest, and E.C. Whipple Jr., "Comment on Low Energy Electron Measurements in the Jovian Magnetosphere," *Geophys. Res. Lett.*, **4**: 247, 1977.
- Grebowski, R. and T. Fischer, "Theoretical Density Distribution of Plasma Around a Cylinder," *Planet. Space Sci.*, **23**: 287–304, 1975.
- Gringauz, K.I. and M.Kh. Zelikman, "Measurement of the Concentration of Positive Ions Along the Orbit of an Artificial Satellite," *Uspekhi Fiz. Nauk*, **63**: 239–252, 1957; (translated in *The Russian Literature of Satellites, Part II*, International Physical Index, New York, 133–147, 1958.)
- Gringauz, K.I., V.V. Bezrukikh, and V.D. Ozerov, "Measurements of the Concentration of Positive Ions in the Ionosphere by Ion Traps on the Third Soviet Earth Satellite," *Iskusstv. Sputniki Zemli*, **6**: 63–100, 1961.
- Gross, B. and S.V. Nablo, "High Potentials in Electron-Irradiated Dielectric," *J. Appl. Phys.*, **38**: 2272–2275, 1967.
- Guernsey, R.L. and J.H.M. Fu, "Potential Distributions Surrounding a Photo-Emitting Plate in a Dilute Plasma," *J. Geophys. Res.*, **75**: 3193–3199, 1970.
- Gurevich, A.V. and Ya.S. Dimant, "Flow of a Rarefied Plasma Around a Disk," *Geomagn. Aeron.*, Engl. Transl., **15**: 183–190, 1975.
- Gurevich, A.V. and L.P. Pitaevskii, "Non-Linear Dynamics of Rarefied Gas," *Prog. Aerospace Sci.*, **16**: 227, 1975.
- Gurevich, A.V., L.V. Pariiskaya, and L.P. Pitaevskii, "Self-Similar Motion of Rarefied Plasma," *Sov. Phys. JETP*, Engl. Transl., **22**: 449, 1966.
- Gurevich, A.V., L.V. Pariiskaya, and L.P. Pitaevskii, "Self-Similar Motion of Low Density Plasma," *Sov. Phys. JETP*, Engl. Transl., **27**: 476, 1968.
- Gurevich, A.V., L.V. Pariiskaya, and L.P. Pitaevskii, "Ion Acceleration Upon Expansion of a Rarefied Plasma," *Sov. Phys. JETP*, Engl. Transl., **36**: 274–281, 1973.
- Gurevich, A.V., L.P. Pitaevskii, and V.V. Smirnov, "Ionospheric Aerodynamics," *Sov. Phys. Usp.*, **99**: 595, 1970.
- Hachenberg, O. and W. Brauer, "Secondary Electron Emission from Solids," in *Advances in Electronics and Electron Physics*, edited by L. Martin, **11**: 413–499, Academic Press, New York, 1959.
- Hanson, W.B., D.D. McKibbin, and G.W. Sharp, "Some Ionospheric Measurements with Satellite-Borne Ion Traps," *J. Geophys. Res.*, **69**: 2747–2763, 1964.
- Hanson, W.B., S. Sanatani, D. Zuccaro, and T.W. Floweryday, "Plasma Measurements with the Retrading Potential Analyzer on OGO 6," *J. Geophys. Res.*, **75**: 5483–5501, 1970.
- Henderson, C.L. and U. Samir, "Observations of the Disturbed Region Around an Ionospheric Spacecraft," *Planet. Space Sci.*, **15**: 1499–1513, 1967.
- Hendrickson, R.A., "The Electron Echo Experiment, Observations of the Charge Neutralization of the Rocket and Analysis of the Echo from Electrons Artificially Injected into the Magnetosphere," *Tech. Report CR-160*, School Physics and Astronomy, University of Minnesota, Minneapolis, 1972.
- Hess, W.N., "Generation of an Artificial Aurora," *Science*, **164**: 1512, 1969.
- Hinteregger, H.E., "Combined Retarding Potential Analysis of Photoelectrons and Environment Charged Particles up to 234 km," *Space Res.*, **1**: 304–327, 1960.
- Inouye, G.T., "Spacecraft Potentials in a Substorm Environment," in *Spacecraft Charging by Magnetospheric Plasma*, (*Prog. Astronaut. Aeronaut.*, **42**) edited by A. Rosen, 103–120, MIT Press, Cambridge, Mass., 1976.
- Jacobsen, T.A. and N.C. Maynard, "Evidence for Significant Spacecraft Charging by an Electron Accelerator at Ionospheric Altitudes," *Planet. Space Sci.*, **28**: 291–307, 1980.
- Jastrow, R. and C.A. Pearce, "Atmospheric Drag on the Satellite," *J. Geophys. Res.*, **62**: 413–423, 1957.
- Jemiola, J.M., *Proceedings of the USAF/NASA International Spacecraft Contamination Conference*, AFML TR-78-190/NASA CP-2039, 1978.
- Jemiola, J.M., "Spacecraft Contamination: A Review," in *Space Systems and Their Interactions with Earth's Space Environment*, (*Prog. Astronaut. Aeronaut.*, **71**) edited by H.B. Garrett and C.P. Pike, 680–706, AIAA Press, New York, 1980.
- Jew, H., "Numerical Studies of the Rarefied Plasma Interaction at Meso-Thermal Speeds," Ph.D. Thesis, University of Michigan, Ann Arbor, Mich., 1968.
- Jew, H., "Reply," *J. Geophys. Res.*, **78**: 6829, 1973.
- Johnson, B., J. Quinn, and S.E. DeForest, "Spacecraft Charging on ATS-6," in *Effect of the Ionosphere on Space and Terrestrial Systems*, edited by John Goodman, U.S. Government Printing Office, Washington, D.C., 322–327, 1978.
- Johnson, C.Y. and E.B. Meadows, "First Investigation of Ambient Positive-Ion Composition to 219 km by Rocket-Borne Spectrometer," *J. Geophys. Res.*, **60**: 193–203, 1955.
- Jung, B., "The Origin of Solid Particles in Interstellar Space," *Astron. Nach.*, **263**: 426, 1937.
- Kasha, M.A., *The Ionosphere and its Interaction with Satellites*, Gordon and Breach, New York, 1969.
- Katz, I., D.E. Parks, S. Wang, and A. Wilson, "Dynamic Modeling of Spacecraft in a Collisionless Plasma," in *Proceedings of the Spacecraft Charging Technology Conference*, edited by C.P. Pike and R.R. Lovell, AFGL TR-77-0051/TMX-73537, ADA045459, 319–330, 1977.
- Katz, I., J.J. Cassidy, M.J. Mandell, G.W. Schnuelle, P.G. Steen, and J.C. Roche, "The Capabilities of the NASA Charging Analyzer Program," in *Spacecraft Charging Technology—1978*, edited by R.C. Finke and C.P. Pike, NASA CP-2071/AFGL TR-79-0082, ADA045459, 101–122, 1979.
- Kennerud, K.L., "High Voltage Solar Array Experiments," *NASA CR-131280*, Boeing Co., Seattle, March 1974.
- Knott, K., "The Equilibrium Potential of a Magnetospheric Satellite in an Eclipse Situation," *Planet. Space Sci.*, **20**: 1137–1146, 1972.

CHAPTER 7

- Knott, K., "Payload of the 'GEOS' Scientific Geostationary Satellite," *ESA Sci. Tech. Rev.*, **1**: 173-196, 1975.
- Knudsen, W.C., "Evaluation and Demonstration of the Use of Retarding Potential Analyzers for Measuring Several Ionospheric Quantities," *J. Geophys. Res.*, **71**: 4669, 1966.
- Knudsen, W.C. and G.W. Sharp, "Ion Temperatures Measured Around a Dawn-Dusk Auroral-Zone Satellite Orbit," *J. Geophys. Res.*, **72**: 1061-1072, 1967.
- Koons, H.C., "Characteristics of Electrical Discharges on the P78-2 Satellite (SCATHA)," Paper 80-0333, AIAA 18th Aerospace Sciences Meeting, AIAA Press, New York, 1980.
- Krassovsky, V.I., "Exploration of the Upper Atmosphere with the Help of the Third Soviet Sputnik," *Proc. IRE*, **47**: 289-196, 1959.
- Kunemann, B., "The Collisionless Flow of Unmagnetized Plasma Around Bodies, 1," *J. Plasma Phys.*, **20**: 17, 1978.
- Kurt, P.G. and V.I. Moroz, "The Potential of a Metal Sphere in Interplanetary Space," *Iskusstvennye Sputniki Zemli*, **7**: 78-88, 1961; (translated in *Planet. Space Sci.*, **9**: 259-268, 1962).
- Laframboise, J.G., "Theory of Spherical and Cylindrical Langmuir Probes in a Collisionless Maxwellian Plasma at Rest," *Report 100*, University of Toronto Institute of Aerospace Studies, Canada, 1966.
- Laframboise, J.B. and E.C. Whipple Jr., Comments on paper by Uri Samir and Howard Jew, "Comparison of Theory with Experiment for Electron Density Distribution in the Near Wake of an Ionospheric Satellite," *J. Geophys. Res.*, **78**: 6827-6828, 1973.
- Laframboise, J.G., R. Godard, and S.M.L. Prokopenko, "Numerical Calculations of High-Altitude Differential Charging: Preliminary Results," in *Spacecraft Charging Technology—1978*, edited by R.C. Finke and C.P. Pike, NASA CP-2071/AFGL TR-79-0082, ADA084626, 188-196, 1979.
- Langmuir, I., "The Interaction of Electron and Positive Ion Spacecharge in Cathode Sheaths," *Phys. Rev.*, **33&34**, 1929 (reprinted in *Collected Works of Irving Langmuir*, edited by G. Suits, **5**, MacMillan, New York, 1961).
- Langmuir, I., and K.B. Blodgett "Currents Limited by Space Charge Between Concentric Spheres," *Phys. Rev.*, **24**: 49, 1924.
- Lehnert, B., "Electrodynamic Effects Connected with the Motion of a Satellite of the Earth," *Tellus*, **3**: 408-409, 1956.
- Liemohn, H.B., "Induced Charging of Shuttle Orbiter by High Electron-Beam Currents," in *Proceedings of the Spacecraft Charging Technology Conference*, edited by C.P. Pike and R.R. Lovell, AFGL TR-77-0051/NASA TMX-73537, ADA045459, 271-286, 1977.
- Linson, L.M., "Current-Voltage Characteristics of an Electron-Emitting Satellite in the Ionosphere," *J. Geophys. Res.*, **74**: 2368-2375, 1969.
- Liu, V.C. and H. Jew, "Near Wake of the Rarefield Plasma Flows at Mesothermal Speeds," *Paper 68-169*, AIAA Press, New York, 1968.
- Liu, V.C., "Ionospheric Gas Dynamics of Satellites and Diagnostic Probes," *Space Sci. Rev.*, **9**: 423, 1969.
- Lucas, A.A., "Fundamental Processes in Particle and Photon Interactions with Surfaces," in *Photon and Particle Interactions with Surfaces in Space*, edited by R.J.L. Gard, 3-21, D. Reidel, Dordrecht, Holland, 1973.
- Manka, R.H., "Plasma and Potential at the Lunar Surface," in *Photon and Particle Interactions with Surfaces in Space*, edited by R.J.L. Gard, D. Reidel, Dordrecht, Holland, 347-367, 1973.
- Massaro, M.J., T. Green, and D. Ling, "A Charging Model for Three-Axis Stabilized Spacecraft," *Proceedings of the Spacecraft Charging Conference*, edited by C.P. Pike and R.R. Lovell, AFGL TR-77-0051/NASA TMX-73537, ADA045459, 237-270, 1977.
- Mazzella, A., E. Tobenfeld, and A.G. Rubin, "AFSIM—An Air Force Satellite Interactions Model," AFGL TR-79-0138, ADA078032, 1979.
- McCoy, J.E., A. Konradi, and O.K. Garriott, "Current Leakage for Low Altitude Satellites," in *Space Systems and Their Interactions with Earth's Space Environment*, *Prog. Astronaut. Aeronaut.*, edited by H.B. Garrett and C.P. Pike, **71**: 523-553, AIAA Press, New York, 1980.
- McPherson, D.A. and W.R. Schober, "Spacecraft Charging at High Altitudes: The SCATHA Satellite Program," in *Spacecraft Charging by Magnetospheric Plasmas*, *Prog. Astronaut. Aeronaut.*, edited by A. Rosen, **47**: 15-30 MIT Press, Cambridge, Mass., 1976.
- Medicus, G., "Theory of Electron Collection of Spherical Probes," *J. Appl. Phys.*, **32**: 2512-2520, 1961.
- Meulenberg, A. Jr., "Evidence for a New Discharge Mechanism for Dielectrics in a Plasma," in *Spacecraft Charging by Magnetospheric Plasmas*, *Prog. Astronaut. Aeronaut.*, edited by A. Rosen, **47**: 237-246, MIT Press, Cambridge, Mass., 1976.
- Mizera, P.F., "Natural and Artificial Charging" Results from the Satellite Surface Potential Monitor Flown on P78-2," *Paper 80-0334*, AIAA 18th Aerospace Sciences Meeting, AIAA Press, New York, 1980.
- Mizera, P.F., E.R. Schnauss, R. Vandre, and E.G. Mullen, "Description and Charging Results from the RSPM," in *Spacecraft Charging Technology—1978*, edited by R.C. Finke and C.P. Pike, NASA CP-2071/AFGL TR-79-0082, ADA084626, 91-100, 1979.
- Montgomery, M.D., J.R. Ashbridge, S.J. Bame, and E.W. Hones, "Low-Energy Electron Measurements and Spacecraft Potential: Vela 5 and Vela 6," in *Photon and Particle Interactions with Surfaces in Space*, edited by R.J.L. Gard, 247-262, D. Reidel, Dordrecht, Holland, 1973.
- Mott-Smith, H.M. and I. Langmuir, "The Theory of Collectors in Gaseous Discharges," *Phys. Rev.*, **28**: 727-763, 1926.
- Mullen, E.G. and M.S. Gussenhoven, "SCATHA Environmental Atlas," AFGL TR-83-0002, ADA131456, 1983.
- Mullen, E.G., M.S. Gussenhoven, and H.B. Garrett, "A 'Worst Case' Spacecraft Environment as Observed by SCATHA on 24 April 1979," AFGL TR-81-0231, ADA108680, 1981.
- Narcisi, R.S., A.D. Bailey, and L. Della Lucca, "Composition Measurements of Negative Ions in the D and

CHARGING OF SPACECRAFT SURFACES

- Lower E Regions (Abstract)," *Eos Trans. AGU*, **49**: 149, 1968.
- Nanevicz, J.E. and R.C. Adamo, "Occurrence of Arcing and Its Effects on Space Systems," in *Space Systems and Their Interactions with Earth's Space Environment*, (*Prog. Astronaut. Aeronaut.*, **71**) edited by H.B. Garrett and C.P. Pike, 252-275, AIAA Press, New York, 1980.
- Norman, K., and R.M. Freeman, "Energy Distribution of Photoelectron Emitted from a Surface on the OGO-5 Satellite and Measurements of Satellite Potential," in *Photon and Particle Interactions with Surfaces in Space*, edited by R.J.L. Grard, 231-246, D. Reidel, Dordrecht, Holland, 1973.
- Olsen, R.C. "Differential and Active Charging Results from the ATS Spacecraft," Ph.D. Thesis, University of California, San Diego, 1980.
- O'Neil, R.R., F. Bien, D. Burt, J.A. Sandock, and A.T. Stair, "Summarized Results of the Artificial Auroral Experiment, Precede," *J. Geophys. Res.*, **83**: 3273, 1978a.
- O'Neil, R.R., W.P. Reidy, J.W. Carpenter, R.N. Davis, D. Newell, J.C. Ulwick, and A.T. Stair, "Excede 2 Test, An Artificial Auroral Experiment: Ground-based Optical Measurements," *J. Geophys. Res.*, **83**: 3281, 1978b.
- Opik, E.J., "Interplanetary Dust and Terrestrial Accretion of Meteoric Matter," *Irish Astron. J.*, **4**: 84, 1956.
- Opik, E.J., "Particle Distribution and Motion in a Field of Force," in *Interactions of Space Vehicles with an Ionized Atmosphere*, edited by S.F. Singer, 3-60, Pergamon Press, New York, 1965.
- Parker, L.W., "Computer Solutions in Electrostatic Probe Theory," Mt. Auburn Res. Associates, Inc., Newton, Mass., AFAL TR-72-222, 1973.
- Parker, L.W., "Computer Method for Satellite Plasma Sheath in Steady-State Spherical Symmetry," Lee W. Parker, Inc., Concord, Mass., AFCRL-TR-75-0410, ADA015066, July 1975.
- Parker, L.W., "Computation of Collisionless Steady State Plasma Flow Past a Charged Disk," *NASA CR-144159*, 1976a.
- Parker, L.W., "Theory of Electron Emission Effects in Symmetric Probe and Spacecraft Sheaths," Lee W. Parker, Inc., Concord, Mass., AFGL-TR-76-0294, A037538, 1976b.
- Parker, L.W., "Calculation of Sheath and Wake Structure about a Pillbox-Shaped Spacecraft in a Flowing Plasma," in *Proceedings of the Spacecraft Charging Technical Conference*, edited by C.P. Pike and R.R. Lovell, AFGL-TR-77-0051/NASA TMX-73537, ADA045459, 331-366, 1977.
- Parker, L.W., "Differential Charging and Sheath Asymmetry of Nonconducting Spacecraft Due to Plasma Flow," *J. Geophys. Res.*, **83**: 4873-4876, 1978a.
- Parker, L.W., "Potential Barriers and Asymmetric Sheaths Due to Differential Charging of Nonconducting Spacecraft," AFGL-TR-78-0045, ADA053618, 1978b.
- Parker, L.W., "Plasma Sheath Effects and Voltage Distributions of Large High Power Satellite Solar Arrays," in *Spacecraft Charging Technology—1978*, edited by R.C. Finke and C.P. Pike, NASA CP-2071/AFGL TR 79-0082 ADA084626, 341-375, 1979.
- Parker, L.W., "Plasmasheath-Photosheath Theory for Large High-Voltage Space Structures," in *Space Systems and Their Interactions with Earth's Space Environment*, (*Prog. Astronaut. Aeronaut.*, **71**) edited by H.B. Garrett and C.P. Pike, 477-522, AIAA Press, New York, N.Y., 1980.
- Parker, L.W., and B.L. Murphy, "Potential Buildup on an Electron-Emitting Ionospheric Satellite," *J. Geophys. Res.*, **72**: 1631, 1967.
- Parker, L.W., and E.C. Whipple, Jr., "Theory of a Satellite Electrostatic Probe," *Ann. Physics*, **44**: 126-161, 1967.
- Parker, L.W., and E.C. Whipple, Jr., "Theory of Spacecraft Sheath Structure, Potential, and Velocity Effects on Ion Measurements by Traps and Mass Spectrometers," *J. Geophys. Res.*, **75**: 4720, 1970.
- Parks, D.E., and I. Katz, "Charging of a Large Object in Low Polar Earth Orbit," in *Proceedings USAF/NASA Spacecraft Charging Technical Conference, III*, 1981.
- Pike, C.P. and M.H. Bunn, *Spacecraft Charging by Magnetospheric Plasmas*, (*Prog. Astronaut. Aeronaut.*, **47**) edited by A. Rosen, 45-60, MIT Press, Cambridge, Mass., 1976.
- Pike C.P., and R.R. Lovell (eds.), *Proceedings of the Spacecraft Charging Technology Conference*, AFGL-TR-77-0051/NASA TMX-73537, 1977.
- Prokopenko, S.M.L., and J.G. Laframboise, "Prediction of Large Negative Shaded-side Spacecraft Potentials," in *Proceedings of the Spacecraft Charging Technology Conference*, edited by C.P. Pike and R.R. Lovell, AFGL-TR-77-0051/NASA, TMX-73537, ADA045459, 369-387, 1977.
- Prokopenko, S.M.L., and J.G. Laframboise, "High-Voltage Differential Charging of Geostationary Spacecraft," *J. Geophys. Res.*, **85**: 4125-4131, 1980.
- Purvis, C.K., "Configuration Effects on Satellite Charging Response," Paper 80-0040, *AIAA 18th Aerospace Science Conference*, 1980.
- Purvis, C.K., and R.O. Bartlett, "Active Control of Spacecraft Charging," in *Space Systems and Their Interactions With the Earth's Space Environment*, (*Prog. Astronaut. Aeronaut.*, **71**) edited by H.B. Garrett and C.P. Pike 299-317, AIAA Press, New York, N.Y., 1980.
- Purvis, C.K., H.B. Garrett, A. Whittlesey, and N.J. Stevens, *Handbook of Design Guidelines for Assessing and Controlling Spacecraft Charging Effects*, NASA Lewis Research Center, NASA TP 2361, September 1984.
- Purvis, C.K., N.J. Stevens, and J.C. Oglebay, "Charging Characteristics of Materials: Comparison of Experimental Results with Simple Analytical Models," in *Proceedings Spacecraft Charging Conference*, edited by C.P. Pike and R.R. Lovell, AFGL-TR-77-0051/NASA TMS-73537 ADA045459, 459-486, 1977.
- Reasoner, D.L., W. Lennartsson, and C.R. Chappell, "Relationship Between ATS-6 Spacecraft Charging Occurrences and Warm Plasma Encounters," in *Spacecraft Charging by Magnetospheric Plasmas*, (*Prog. Astronaut. Aeronaut.*, **47**) edited by A. Rosen, 89-102, MIT Press, Cambridge, Mass., 1976.
- Reddy, B.M., L.H. Brace, and J.A. Findlay, "The Ionosphere at 640 Kilometers on Quiet and Disturbed Days," *J. Geophys. Res.*, **72**: 2709-2727, 1967.

CHAPTER 7

- Reiff, P.H., J.W. Freeman, and D.L. Cooke, "Environmental Protection of the Solar Power Satellite," in *Space Systems and Their Interactions With the Earth's Space Environment*, (*Prog. Astronaut. Aeronaut.*, **71**) edited by H.B. Garrett and C.P. Pike, 554–576, AIAA Press, New York, 1980.
- Robinson, P.A., Jr., and A.B. Holman, "Pioneer Venus Spacecraft Charging Model," in *Proceedings Spacecraft Charging Technical Conference*, edited by C.P. Pike and R.R. Lovell, AFGL-TR-77-0051/NASA TMX-73537, 297–308, ADA045459, 1977.
- Roche, J.C., and C.P. Purvis, "Comparison of NASCAP Predictions with Experimental Data," in *Spacecraft Charging Technology—1978*, edited by R.C. Finke and C.P. Pike, NASA CP-1072/AFGL-TR-79-0082, ADA084626, 144–157, 1979.
- Rosen, A. (ed.), *Spacecraft Charging by Magnetospheric Plasmas*, (*Prog. Astronaut. Aeronaut.*, **47**) MIT Press, Cambridge, Mass., 1976.
- Rosen, A., R.W. Fredericks, Inouye, N.L. Saunders, F.L. Scarf, W.M. Greenstadt, J.L. Vogl, and J.M. Sellen, "RGA Analysis: Findings Regarding Correlation of Satellite Anomalies with Magnetospheric Substorms and Laboratory Test Results," *Report 09760-7020-R0-00*, Aug 1972, TRW Systems Group, Redondo Beach, Calif.
- Rothwell, P.L., A.G. Rubin, A.L. Pavel, and L. Katz, "Simulation of the Plasma Sheath Surrounding a Charged Spacecraft," in *Spacecraft Charging by Magnetospheric Plasmas*, (*Prog. Astronaut. Aeronaut.*, **47**) edited by A. Rosen, 121–134, MIT Press, Cambridge, Mass., 1976.
- Rothwell, P.L., A.G. Rubin, and G.K. Yates, "A Simulation Model of Time-Dependent Plasma-Spacecraft Interactions," *Proc. Spacecraft Charging Conf.*, edited by C.P. Pike and R.R. Lovell, AFGL-TR-77-0051/NASA TMS-73537, ADA045459, 381–412, 1977.
- Rubin, A.G., P.L. Rothwell, and G.K. Yates, "Reduction of Spacecraft Charging Using Highly Emissive Surface Materials," *Proceedings of the 1978 Symposium on the Effects of the Ionosphere on Space and Terrestrial Systems*, Naval Research Laboratory, Washington, D.C., 1978.
- Rubin, A.G. et al., I. Katz, M. Mandell, G. Schnuelle, P. Steen, D. Parks, J. Cassidy, and J. Roche, "A Three-Dimensional Spacecraft Charging Computer Code," in *Space Systems and Their Interactions With the Earth's Space Environment*, (*Prog. Astronaut. Aeronaut.*, **71**) edited by H.B. Garrett and C.P. Pike, 318–336, AIAA Press, New York, 1980.
- Sagalyn, R.C., and W.J. Burke, "INJUN 5 Observations of Vehicle Potential Fluctuations at 2500 km," in *Proceedings of Spacecraft Charging Technology Conference*, edited by C.P. Pike and R. R. Lovell, AFGL TR-77-0051, NASA TMS-73537, 67–80, 1977.
- Sagalyn, R.C., M. Smiddy, and J. Wisnia, "Measurement and Interpretation of Ion Density Distributions in the Daytime F Region," *J. Geophys. Res.*, **63**: 199–211, 1963.
- Samir, U., "Charged Particle Distribution in the Nearest Vicinity of Ionospheric Satellites - Comparison of the Main Results from the Ariel I, Explorer 31, and Gemini-Agena 10 Spacecraft," in *Photon and Particle Interactions with Surfaces in Space*, edited by R.J.L. Grard, 193–220, D. Reidel, Dordrecht, Holland, 1973.
- Samir, U., and H. Jew, "Comparison of Theory with Experiment for Electron Density Distribution in the Near Wake of an Ionospheric Satellite," *J. Geophys. Res.*, **77**: 6819–6827, 1972.
- Samir, U., and G.L. Wrenn, "The Dependence of Charge and Potential Distribution Around a Spacecraft on Ionic Composition," *Planet. Space Sci.*, **17**: 693, 1969.
- Samir, U., L.H. Brace, and H.C. Brinton, "About the Influence of Electron Temperature and Relative Ionic Composition on Ion Depletion in the Wake of the AE-C Satellite," *Geophys. Res. Lett.*, **6**: 101–104, 1979a.
- Samir, U., R. Gordon, L. Brau, and R. Theis, "The Near-Wake Structure of the Atmosphere Explorer C. (AE-C) Satellite: A Parametric Investigation," *J. Geophys. Res.*, **84**: 513–525, 1979b.
- Samir, U., Y.J. Kaufmann, L.H. Brace, and H.C. Brinton, "The Dependence of Ion Density in the Wake of the AE-C Satellite on the Ratio of Body Size to Debye Length in an (O^+)-Dominated Plasma," *J. Geophys. Res.*, **85**: 1769–1772, 1980.
- Sanders, N.L. and G.T. Inouye, "Secondary Emission Effects on Spacecraft Charging: Energy Distribution Considerations," in *Spacecraft Charging Technology—1978*, edited by R.J. Finke and C.P. Pike, NASA CP-2071/AFGL TR-79-0082, 747–755, 1979.
- Schnuelle, G. W. et al., D.E. Parks, I. Katz, M.J. Mandell, P.G. Steen, J.J. Cassidy, and A. Rubin, "Charging Analysis of the Scatha Satellite," in *Spacecraft Charging Technology—1978*, edited by R.C. Finke and C.P. Pike, NASA CP-2071/AFGL TR-0087, 123–143, 1979.
- Schnuelle, G.W., P.R. Stannard, I. Katz, and M.J. Mandell, "Stimulation of the Charging Response of the SCATHA (P78-2) Satellite," in *Proceedings of the USAF/NASA Spacecraft Charging Technical Conference III*, 1981.
- Schroder, H., "Spherically Symmetric Model of the Photoelectron Sheath for Moderately Large Plasma Debye Lengths," in *Photon and Particle Interactions with Surfaces in Space*, edited by R.J.L. Grard, 51–58, D. Reidel, Dordrecht, Holland, Mass., 1973.
- Schwenn, R., H. Rosenbauer, and K.H. Muhlhauser, "The Solar Wind during STIP II Interval: Stream Structures, Boundaries, Shocks, and Other Features as Observed by the Plasma Instruments on Helios-1 and Helios-2," *Contributed Papers to the Study of Travelling Interplanetary Phenomena 1977*, edited by M.A. Shea, D.F. Smart and S.T. Wu, AFGL TR-77-0309, ADA056931, 1977.
- Scudder, J.D., E.C. Sittler, Jr., and H.S. Bridge, "A Survey of the Plasma Electron Environment of Jupiter: A View from Voyager," *J. Geophys. Res.*, **86**: 8157, 1981.
- Shaw, R.R., J.E. Nanevich, and R.C. Adamo, "Observations of Electrical Discharges Caused by Differential Satellite Charging," *Spacecraft Charging by Magnetospheric Plasmas*, AIAA (*Prog. Astronaut. Aeronaut.*, **47**) edited by A. Rosen, 61–76, 1976.
- Shawhan, S.D., R.F. Hubbard, G. Joyce, and D.A. Gurnett, "Sheath Acceleration of Photoelectrons by Jupiter's

- Satellite Io," in *Photon and Particle Interactions with Surfaces in Space*, edited by R.J.L. Grard, 504–414, D. Reidel, Dordrecht, Holland, 1973.
- Singer, S.F. (ed.), *Interactions of Space Vehicles with an Ionized Atmosphere*, Pergamon Press, New York, 1965.
- Soop, M., "Report on Photosheath Calculations for the Satellite GEOS," *Planet. Space Sci.*, **20**: 859, 1972.
- Soop, M., "Numerical Calculations of the Perturbation of an Electric Field Around a Spacecraft," in *Photon and Particle Interactions with Surfaces in Space*, edited by R.J.L. Grard, 127, D. Reidel, Dordrecht, Holland, 1973.
- Spencer, N.W., L.H. Brace, G.R. Corigan, D.R. Tausch, and H. Nieman, "Electron and Molecular Nitrogen Temperature and Density in the Thermosphere," *J. Geophys. Res.*, **70**: 2665–2698, 1965.
- Spitzer, L., Jr., "The Dynamics of the Interstellar Medium," *Astrophys. J.*, **93**: 369–379, 1941.
- Spitzer, L., Jr., "The Temperature of Interstellar Material," *Astrophys. J.*, **107**: 6–33, 1948.
- Spitzer, L., Jr., and M.P. Savedoff, "The Temperature of Interstellar Matter, III," *Astrophys. J.*, **111**: 593–608, 1950.
- Sternglass, E.J., "Backscattering of Kilovolt Electrons from Solids," *Phys. Rev.*, **95**: 345, 1954.
- Sternglass, E.J., "Theory of Secondary Electron Emission by High Speed Ions," *Phys. Res.*, **108**: 1–12, 1957.
- Stevens, N.J., "Space Environment at Interactions with Biased Spacecraft Surfaces," in *Space Systems and Their Interactions With the Earth's Space Environment*, (*Prog. Astronaut. Aeronaut.*, **71**) edited by H.B. Garrett and C.P. Pike 455–476, AIAA Press, New York, N.Y., 1980.
- Stevens, N.J., and C.K. Purvis, "NASCAP Modeling Computations on Large Optics Spacecraft in Geosynchronous Substorm Environments," *NASA TM-81395*, 1980.
- Stevens, N.J., J.V. Staskus, J.C. Roche, and P.F. Mizera, "Initial Comparison of SSPM Ground Test Results and Flight Data to NASCAP Simulations," *NASA TM-81394*, 1980a.
- Stevens, N.J., J.V. Staskus, and J.C. Roche, "Initial Comparison of SSPM Ground Test Results and Flight Data to NASCAP Simulations," *NASA TM-81314*, 1980c.
- Suh, P.K., and M.C. Stauber, "Photoelectron Drift and Multiplication due to Surface Potential Gradient; Application to Solar Power Arrays," Paper 80-0044, AIAA 18th Aerospace Sciences Conference, AIAA, New York, 1980.
- Taylor, H.A., Jr., H.C. Brinton, and C.R. Smith, "Positive Ion Composition in the Magnetionosphere Obtained from the OGO-A Satellite," *J. Geophys. Res.*, **70**: 5769–5781, 1965.
- Treadway, M.J., C.E. Mallon, T.M. Flanagan, R. Denson, and E.P. Wenaas, "The Effects of High-Energy Electrons on the Charging of Spacecraft Dielectrics," *IEEE Trans. Nuc. Sci.*, **NS-26**, (6), 5102–5106, 1979.
- Tsien, H.S., "Superaerodynamics, Mechanics of Rarefied Gases," *J. Aero. Sci.*, **13**, 653–664, 1946.
- Tsipouras, P., and H.B. Garrett, "Spacecraft Charging Model 2 Maxwellian Approximation," *AFGL TR-79-0153*, ADA077907, 1979.
- Walker, E.H., "Plasma Sheath and Screening Around a Stationary Charged Sphere and a Rapidly Moving Charged Body," in *Interactions of Space Vehicles with an Ionized Atmosphere*, edited by S.F. Singer, 61–162, Pergamon Press, New York, 1965.
- Walker, E.H., "Plasma Sheath and Screening of Charged Bodies," in *Photon and Particle Interactions with Surfaces in Space*, edited by R.J.L. Grard, D. Reidel, Dordrecht, Holland, 73–89, 1973.
- Whipple, E.C., Jr., "The Ion-Trap Results in the 'Exploration of the Upper Atmosphere with the Help of the Third Soviet Sputnik,'" *IRE Trans.*, **47**: 2023–2024, 1959.
- Whipple, E.C., Jr., "The Equilibrium Electric Potential of a Body in the Upper Atmosphere," *NASA X-615-65-296*, 1965.
- Whipple, E.C., Jr., "Theory of the Spherically Symmetric Photoelectron Sheath: A Thick Sheath Approximation and Comparison with the ATS-6 Observations of a Potential Barrier," *J. Geophys. Res.*, **81**: 601–607, 1976a.
- Whipple, E.C., Jr., "Observation of Photoelectrons and Secondary Electrons Reflected from a Potential Barrier in the Vicinity of ATS-6," *J. Geophys. Res.*, **81**: 715, 1976b.
- Whipple, E.C., Jr., "Modeling of Spacecraft Charging," in *Proceedings of Spacecraft Technical Conference*, edited by C.P. Pike and R.R. Lovell, AFGL TR-77-0051/NASA TMX-73537, ADA045459, 225–236, 1977.
- Whipple, E.C., Jr., and L.W. Parker, "Theory of an Electron Trap on a Charged Spacecraft," *J. Geophys. Res.*, **74**: 2962–2971, 1969a.
- Whipple, E.C., Jr., and L.W. Parker, "Effects of Secondary Electron Emission on Electron Trap Measurements in the Magnetosphere and Solar Wind," *J. Geophys. Res.*, **74**: 5763, 1969b.
- Whipple, E.C., Jr., J.M. Warnock, and R.H. Winkler, "Effect of Satellite Potential on Direct Ion Density Measurement through the Plasmopause," *J. Geophys. Res.*, **79**: 179–186, 1974.
- Wildman, P.J.L., "Dynamics of a Rigid Body in the Space Plasma," in *Space Systems and Their Interactions With Earth's Space Environment*, (*Prog. Astronaut. Aeronaut.*, **71**) edited by H.B. Garrett and C.P. Pike, 633–661, AIAA Press, New York, 1980.
- Williamson, P.R., W. Denig, P.M. Banks, and W.J. Raitt, "Vehicle Potential Measurements Using a Mother-Daughter Tethered Rocket (Abstract)," *Eos Trans. AGU*, **61**: 1068, 1981.
- Willis, R.F., and D.K. Skinner, "Secondary Electron Emission Yield Behaviors of Polymers," *Solid State Commun.*, **13**: 685, 1973.
- Winkler, J.R., "A Summary of Recent Results Under the 'Echo' Program for the Study of the Magnetosphere by Artificial Electron Beams," *Cosmic Phys. Tech. Report 168*, School of Physics and Astronomy, University of Minnesota, Minneapolis, September 1976.
- Winkler, J.R., "The Application of Artificial Electron Beams to Magnetospheric Research," *Rev. Geophys. Space Phys.*, **18**: 659–682, 1980.
- Zonov, Yu, V., "On the Problem of the Interaction Between a Satellite and the Earth's Atmosphere and the Earth's Magnetic Field," *Iskusstvennyye Sputniki Zemli*, **3**, 1959, (NASA Tech. Transl. TTF-37).